AMERICAN UNIVERSITY OF BEIRUT

Method for Deriving the Complex Infrared Dielectric Function of Amorphous Thin Films from Infrared Reflectivity Spectroscopy

by
MARWA YOUSSEF DAKIK

A thesis
submitted in partial fulfillment of the requirements
for the degree of Master of Sciences
to the Department of Physics
of the Faculty of Art and Sciences
at the American University of Beirut

Beirut, Lebanon
September 2020

AMERICAN UNIVERSITY OF BEIRUT

Method for Deriving the Complex Infrared Dielectric Function of Amorphous Thin Films from Infrared Reflectivity Spectroscopy

by

MARWA YOUSSEF DAKIK

Approved by:

Dr. Michel Kazan, Associate Professor Physics	Advisor
Dr. Malek Tabbal, Professor Physics	Member of Committee
Dr. Sara Najem, Assistant Professor Physics	Member of Committee

Date of thesis defense: September 14, 2020

AMERICAN UNIVERSITY OF BEIRUT

THESIS RELEASE FORM

Student Name: DAKIK Marwa Youssef
Last First Middle

☑ Master's Thesis ○ Master's Project ○ Doctoral Dissertation

☐ I authorize the American University of Beirut to: (a) reproduce hard or electronic copies of my thesis, dissertation, or project; (b) include such copies in the archives and digital repositories of the University; and (c) make freely available such copies to third parties for research or educational purposes.

☑ I authorize the American University of Beirut, to: (a) reproduce hard or electronic copies of it; (b) include such copies in the archives and digital repositories of the University; and (c) make freely available such copies to third parties for research or educational purposes after:

One ✓ year from the date of submission of my thesis, dissertation or project.
Two ___ years from the date of submission of my thesis , dissertation or project.
Three ___ years from the date of submission of my thesis , dissertation or project.

Signature 16/09/2020
Date

This form is signed when submitting the thesis, dissertation, or project to the University Libraries

Acknowledgements

Foremost, I would like to thank my thesis advisor, Professor Michel Kazan, whose expertise was invaluable in formulating the research questions and methodology. The door to Prof. Kazan office was always open whenever I ran into a trouble spot or had a question about my research or writing.

Besides my advisor, I would like to thank my thesis committee: Prof. Malek Tabbal and Dr. Sara Najem for their encouragement and support in terms of communication and availability.

Getting through my thesis work required more than academic support, and I have many friends and graduate colleagues to thank for listening to and, at times, having to tolerate me over the past three years. I cannot begin to express my gratitude and appreciation for their friendship. *Kafa Alameh*, *Rola Dbouk*, *Ghina Al-Atat*, and *Zeinab Harajli* have been unwavering in their personal and professional support during the time I spent at the University. For many memorable evenings out and in, I must thank my best friend *Nour Meslamani* for being there when needed.

Most importantly, none of this could have happened without my family. I would like to thank my parents and my brother, whose love and guidance are with me in whatever I pursue. Finally, I wish to thank my loving and supportive husband, *Nehmeh*, and my beautiful daughter, *Maryam*, who provide unending inspiration. This thesis stands as a testament to your unconditional love and encouragement.

An Abstract of the Thesis of

Marwa Youssef Dakik for Master of Sciences
Major: Physics

Title: Method for Deriving the Complex Infrared Dielectric Function of Amorphous Thin Films from Infrared Reflectivity Spectroscopy

Although advanced nonlinear optical techniques have demonstrated high potential for examining elementary excitations in semiconductors, infrared reflectivity analysis remains the most quantitative technique because simple theories can be used to describe the material response to an infrared wavelength excitation. Line shape analysis, comparatively rare for non-linear optical spectroscopy, can be carried out to yield quantitative results.

Therefore, our objective in the present thesis is to develop an experimental approach based on infrared spectroscopy for the characterization of the complex infrared dielectric function of amorphous thin films grown on a substrate, which is inaccessible by other means. The proposed approach is based on the analysis of the infrared reflectivity spectrum of the considered film/substrate using a numerical technique combining the Fresnel theory and the Kramers-Kronig conversion theorem.

We used the technique developed to deduce the complex infrared dielectric function of amorphous silicon carbide thin films deposited on silicon at different temperatures and pressure levels using the pulsed laser deposition (PLD) growth technique. The results obtained showed that the growth temperature does not have a significant effect on the dielectric properties of the amorphous films. However, the variation in pressure allows a substantial modification of the real and imaginary parts of the infrared complex dielectric function of the amorphous silicon carbide film.

We believe that the optical technique developed in this work constitutes a non-destructive method for the characterization of relevant infrared properties of amorphous materials, which so far are not clear to materials scientists.

Contents

List of Figures

List of Tables

Chapter 1

ELECTROMAGNETIC WAVES IN SEMICONDUCTORS

By framing previously known experimental results of Coulomb, Gauss, Ampere, and Faraday and by including the notion of displacement current, James Clerk Maxwell released the unified theory of electricity and magnetism in 1873. The argument consists of four fundamental equations, named ***Maxwell's Equations***. The argument states that any electromagnetic field is invariant under time-varying conditions. No matter what the material medium is, Maxwell's equations hold. There are two forms of these equations: the integral and the differential form.

The differential form is beneficial in identifying the electromagnetic field intensities at each point in the given space. On the other hand, the integral structure is useful in explaining the underlying physical concepts.

Specifically, the electromagnetic radiation-matter interaction can be explained using the classical effect of an oscillating electric field on a charge or using the quantum mechanical effect in studying the bandgap and phonons. In this chapter, we will start by discussing the classical approach of the interaction and then shift to the quantum approach.

1.1 Classical Approach:

1.1.1 Electromagnetic waves in free space

Basic electromagnetic behavior is defined by Maxwell's Equations [21]. Their solutions in free space identify undamped transverse waves composed of perpendicular oscillating magnetic and electric fields, which propagate at a constant speed of light. Inside the solid, the interaction between the electromagnetic field and the charges produce damped waves as they transmit energy to the solid. The wave speed of propagation is not constant and depends on the frequency. The

complete classical description of light is embedded in Maxwell's Equations:

$$\nabla \times \mathbf{E} = -\frac{\partial \mathbf{B}}{\partial t} \tag{1.1}$$

$$\nabla \times \mathbf{H} = j + \frac{\partial \mathbf{D}}{\partial t} \tag{1.2}$$

$$\nabla \cdot \mathbf{D} = \rho \tag{1.3}$$

$$\nabla \cdot \mathbf{B} = 0 \tag{1.4}$$

Where:

- E: Electric Field and D: Displacement Vector
- B: Magnetic Field and H: Magnetic Field Strength
- ρ: Charge Density and j: Current Density

1.1.2 Electromagnetic waves in Semiconductors

Unlike free space, semiconductors contain both free charges and bound charges. The free charges in a semiconductor are the conduction electrons and the valence band holes. The bound charges are coated into the lattice structure that includes the host crystal and the inner electrons that are tightly localized at the atomic cores. Thus, Maxwell's Equations are affected by the current and charge density due to the free charges and the bound charge's polarizability. Bound charges in crystal produce polarization $\mathbf{P}$, which is the dipole moment per unit volume. In a homogeneous linear and isotropic medium, the polarization is aligned and proportional to the external electric field $\mathbf{E}$:

$$P = \varepsilon_0 \chi E \tag{1.5}$$

Where:

- ε_0: Electric Permittivity in Free Space
- χ: Susceptibility, a specific property of the material

The relation between the electric Displacement $\mathbf{D}$ of the medium and the electric field $\mathbf{E}$ is called the constitutive relations of the electromagnetic medium:

$$\mathbf{D} = \varepsilon_0 E + P = \varepsilon_0 (1 + \chi) E = \varepsilon_0 \varepsilon_{latt} E \tag{1.6}$$

Where:

- The lattice frequency-dependent dielectric response is defined as:

$$\varepsilon_{latt} = 1 + \chi \tag{1.7}$$

Due to the applied electric field, the current will flow in the material. Ohm's Law describes the proportionality between the current density **j** and the electric field **E**:

$$j = \sigma(w)E \tag{1.8}$$

Where

- $\sigma(w)$: Electric conductivity of the material

Substituting the linear relations **1.6** and **1.8** in Maxwell's Equations **1.1** - **1.4** and eliminating B and H:

$$\nabla^2 E - \nabla(\nabla \cdot E) = \varepsilon_{latt}\varepsilon_0\mu_0\frac{\partial^2 E}{\partial^2 t} + \sigma\mu_0\frac{\partial E}{\partial t} \tag{1.9}$$

Assuming a plane wave solution:

$$E = E_0 e^{i(\mathbf{k}z-\omega t)} \tag{1.10}$$

- E_0: Amplitude of the wave
- ω: angular frequency
- **K**: Wave vector In a non-absorbing medium:

$$\mathbf{k} = \frac{2\pi}{\lambda} = \frac{w}{v} = \frac{nw}{c} \tag{1.11}$$

  - λ: Wavelength inside the medium
  - n: index of refraction
  - v: speed of the wave
  - c: speed of light

Substituting **1.10** into **1.9**:

$$\mathbf{k}^2 - \mathbf{k}(\mathbf{k} \cdot E) = \varepsilon_{latt}\varepsilon_0\mu_0\omega^2 E + i\sigma\mu_0\omega E = \omega^2\varepsilon(\omega)\varepsilon_0\mu_0 E \tag{1.12}$$

The total dielectric response function $\varepsilon(\omega)$ is given by:

$$\varepsilon(\omega) = \varepsilon_{latt}(\omega) + i\frac{\sigma(\omega)}{\varepsilon_0\omega} \tag{1.13}$$

$\varepsilon(\omega)$ is considered the central quantity that specifies the interaction between the electromagnetic wave and semiconductors in the linear limit.

Now, the electric field **E** is expressed in terms of the longitudinal and transverse components:

$$E = E_t\hat{t} + E_k\hat{k} \tag{1.14}$$

- $\hat{t}$: Unit vector in the x-y plane perpendicular to the direction of propagation
- $\hat{k}$: Unit vector along with $\mathbf{k}$

With this decomposition, equation **12** becomes:

$$[\frac{\omega^2}{c^2}\varepsilon(\omega) - \mathbf{k}^2]E_t\hat{t} + \frac{\omega^2}{c^2}\varepsilon(\omega)E_k\hat{k} = 0 \tag{1.15}$$

Since the two terms in equation **1.15** are linearly independent, each term should be set to zero to satisfy the above condition.

Thus the generalized dispersion relation for the transverse wave is:

$$\mathbf{k}^2 = \frac{\omega^2}{c^2}\varepsilon(\omega) \tag{1.16}$$

And the dispersion relation for the longitudinal waves is:

$$\varepsilon(\omega) = 0 \tag{1.17}$$

Due to these derivations, equation **1.11** can be generalized to the absorbing medium where we have a complex refractive index

$$\mathbf{k} = \frac{\tilde{n}\omega}{c} = (n + i\mathbf{k})\frac{\omega}{c} \tag{1.18}$$

- With: $\tilde{n}$ = n + i k

Substitute equation **1.18** back in the wave solution equation **110**:

$$E(z,t) = E_0 e^{\frac{-\mathbf{k}\omega z}{c}} e^{i(\frac{\omega n z}{c} - \omega t)} \tag{1.19}$$

This equation explains the physical meaning of the refractive index and the complex wave-vector. It illustrates that the real part of $\tilde{n}$ is related to wave propagation. Whereas the imaginary part of $\tilde{n}$, k the 'extension coefficient', is linked to an exponential decay of the wave as it enters the medium.

Now, by combining **1.18** and **1.16**, we extract the relation between the complex refractive index and the total dielectric function this way:

$$\tilde{n} = \sqrt{\varepsilon(\omega)} \tag{1.20}$$

Expressing $\varepsilon(\omega)$ as real and imaginary parts, we get:

$$\varepsilon(\omega) = \varepsilon_1 + \varepsilon_2 = \tilde{n}^2 \tag{1.21}$$

The relations between the real and imaginary parts of $\tilde{n}$ and $\varepsilon(\omega)$ can be pulled out using equation **1.16**. The relations are:

$$\begin{aligned} \varepsilon_1 &= n^2 - k^2 \\ \varepsilon_2 &= 2nk \\ n &= \frac{1}{\sqrt{2}}\sqrt{\varepsilon_1 + |\varepsilon|} \\ k &= \frac{1}{\sqrt{2}}\sqrt{-\varepsilon_1 + |\varepsilon|} \end{aligned} \tag{1.22}$$

Therefore, the microscopic optical response of semiconducting materials, determined by the refractive index and the extinction coefficients, can be manipulated by its frequency-dependent dielectric function. The calculation will be cleared when the reflectance spectroscopy of the semiconductor is considered.

1.2 Basic Semiconductor Physics

A crystalline semiconductor is composed of repetitive geometric arrays of atoms. Quantum mechanics explains the energy between the lowest point in the conduction band of a crystalline semiconductor and the highest point in its valence band. This energy difference is called the bandgap that determines the conductivity of materials. The valence electron can absorb heat or light energy, to enable them to jump up into the conduction band. Each electron that moves to the conduction band leaves behind a vacant position-hole. This process is called the electron-hole pair generation.

1.3 Semiconducting materials

As shown in figure 1.1, elements in the periodic table are divided into one of 3 categories:

- Metals: the most abundant category
- Non-metals
- Semi-metals

Metals are considered perfect conductors, whereas non-metals are very good insulators as they do not conduct electricity. However, semi-metals do conduct electricity if the conditions are right. Silicon is playing a crucial role in the electronic industry. Si-based sensors are widely used in the automobile sector. Moreover, thermal radiators that are based on silicon or gallium arsenide semiconductors are essential satellites and aircraft as they dissipate energy. [18]

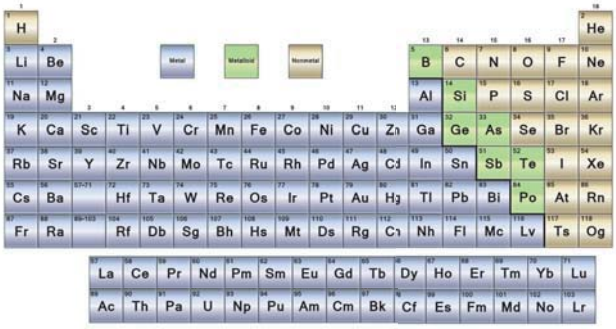

Figure 1.1: Periodic Table

Silicon carbide was first discovered in 1824 by a Swedish scientist, Jons Jacob Berzelius, [2] while Henri Moissan discovered naturally occurring SiC in 1905, he found small hexagonal platelets in a meteorite. In recent years, silicon carbide (SiC) materials have played an essential role in the development of various semiconductor applications due to their unique characteristics, making them suitable materials for devices operating at high power, high frequency, and high temperature. Silicon carbide's ability to function under such extreme conditions is expected to enable some significant improvements in a variety of applications and systems [10]. Silicon carbide is a compound semiconductor composed of silicon (Si) and carbon (C). Naturally, SiC exits in several crystalline structures, called polytypes or polymorphs. The presence of different polytypes indicates that there exists an enormous number of different atomic symmetries and arrangements. The most significant polytypes are the cubic 3C and the hexagonal 4H and 6H phases, all of which have different physical properties. For example, the energy band gap E_G is equal to 2.403, 3.285 and 3.101 eV for 3C, 4H and 6H-SiC respectively [18]. The high value of thermal conductivity k_T is another feature that makes SiC eventually valuable for very high-power electronic devices. The value of k_T varies from 3.2 to 3.7 $Wcm^{-1}K^{-1}$ based on the polytype. It is worth mentioning that SiC has a wider energy bandgap and higher thermal conductivity than Si. Besides, under the impact of a low electric field in semiconductors, the carrier (electron or hole) will reach an average drift velocity $v_d = \mu E$ where μ is the mobility of the charge carrier. In the case of large electric fields, the velocity does not depend on the doping and achieves its saturation value. The values of the SiC polytypes are greater than those measured in Si. Thus SiC turns out to be a perfect candidate for building radio-frequency RF and microwave devices [18].

In contrast, amorphous silicon carbide alloys (a-SiC) play an important role in applications ranging from microelectronic and optoelectronic devices [24] to protective coatings for biocompatible implants [11]. Amorphous silicon carbide is

the most convenient material to either boost the tribological behavior of surfaces (wear resistance and sliding friction) or to improve device reliability and lifetime. The primary justification for the advantages of using a-SiC is the combination of optical and electronic properties and exceptional mechanical characteristics (including its high hardness). These amorphous materials have a complex structure that relies on the atomic scale and/or large scale disorder, as well as hydrogen content and stoichiometry [24]. However, the synthesis of such materials and interpreting their growth mechanisms are necessary for manufacturing devices that could be launched in the mass market.

Crystalline silicon carbide (c-SiC) thin films have been deposited using several synthesis procedures such as Chemical Vapor Deposition [29], Electron Cyclotron Resonance (ECR-CVD) [17], Ion Beam Implantation [25], and Molecular Beam Epitaxy [12]. Pulsed- Laser Deposition (PLD) which is the deposition of the material emitted from a SiC target ablated under vacuum by high power laser pulses, is also another technique to grow epitaxial, polycrystalline SiC and hydrogen-free amorphous a-SiC. PLD method avoids contamination by spurious elements. This is the growth method that is used in our work to synthesize both crystal and amorphous silicon carbide.

1.4 Theoretical Model

The infrared dielectric function determines the intrinsic optical response of any material to infrared radiation. The dielectric function is related to the characteristics of the material's lattice vibrations (phonon modes) and free charge carriers' plasma oscillations.

1.4.1 Phonon Modes

Phonons are the atoms quantized vibrations inside a crystal lattice. In the infrared spectral region, semiconductor crystals are made of a three-dimensional array of atoms that are vibrating at characteristic resonant frequencies, which are defined by the crystal phonon modes. Solving classically the atomic equations of motion, one can extract the dispersion relation (ω as a function of k) of the characteristic normal vibrational modes. The dispersion relations formulate two branches for the atomic displacements, namely, optical and acoustical branches. The phonon modes as well are partitioned into two general classes: optical or acoustic. Each category can be either transverse or longitudinal. Optical modes are atomic vibrations where the vibrations of two different atoms in the same unit cell are out of phase. These vibrations establish a polarization effect across a dynamical oscillating dipole moment which matches to an external oscillating electric field. On the other hand, the acoustical modes outline the vibrations of cells when the two atoms vibrate along a uniform direction. It is worth

mentioning that the optical modes are IR active since they absorb infrared light at their resonant frequencies. Effectively, the infrared active (IR active) modes occur when the coupling between phonon modes and the electrostatic field of the lattice splits between longitudinal and transverse [13]. Thereby, the acoustical branch is divided into longitudinal (LA) and transverse (TA) modes while the optical one splits into longitudinal (LO) and transverse (TO) modes.

The fig. 1.2 shows the displacement of atoms in a direction perpendicular (transverse) and parallel (longitudinal) to the wave propagation for both acoustic and optical modes [14].

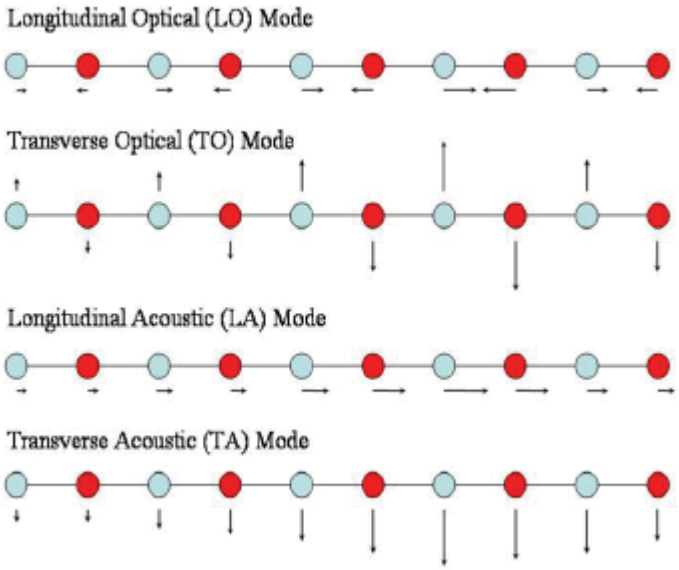

Figure 1.2: :Displacements for acoustic and optical phonon modes of vibrations of two atoms in the unit cell of an ionic crystal

Photons apply only driving forces to the transverse vibrations of the crystal because the electromagnetic waves are transverse. Hence, the longitudinal phonons do not affect the direction of the induced field is perpendicular to the electromagnetic wave. Consequently, resonant absorption takes place when the incoming frequency of light ω is equal to the TO phonon frequency of ω_{TO}. Yet the infrared properties of crystals are controlled by the LO modes.

1.4.2 The Dipole Oscillator Model

Lorentz model, which models the displacement of the atomic dipoles as damped harmonic oscillators, is critical for understanding the optical properties of semiconductors. This model provides a classical characterization of the light-matter interaction, where both are treated as classical objects that abide by the law of

classical mechanics. The equation of motion of the classical damped oscillation with resonance frequency ω_{TO} is:

$$\mu\frac{d^2x}{dt^2} + \mu\Gamma\frac{dx}{dt} + \mu\omega_{TO}^2 x = -eE_0e^{-i\omega t} \tag{1.23}$$

where

- Γ: is the damping rate modeled by a frictional force which is proportional to the velocity
- μ: is the reduced mass of the TO phonon
- E_0: is the electric field amplitude of the light wave

This equation displays a relation between the acceleration, the damping rate, the restoring term, and the driving force exerted by the electric field of light on the right side.

Searching for a solution of the form $x = x(0)e^{-i\omega t}$ provides the displacement amplitude of the positive ions relative to the negative ones:

$$x(0) = \frac{-eE_0}{\mu(\omega_{TO}^2 - \omega^2 - i\Gamma\omega} \tag{1.24}$$

For N number of atoms, the resonant polarization due to the displacement of electrons from their equilibrium position is:

$$\mathbf{P} = -Nex = \frac{-e^2NE_0}{\mu(\omega_{TO}^2 - \omega^2 - i\Gamma\omega)} \tag{1.25}$$

Knowing that $D = \epsilon_0\mathbf{E} + \epsilon_0\chi\mathbf{E} + \mathbf{P}_{resonant}$, the lattice dielectric function is:

$$\epsilon_{latt}(\omega) = 1 + \chi + \frac{e^2N}{\mu\epsilon_0(\omega_{TO}^2 - \omega^2 - i\Gamma\omega)} \tag{1.26}$$

At the two extremities 0 and ∞, the dielectric functions are defined by:

$$\begin{aligned} \epsilon_{latt}(0) &= 1 + \chi + \frac{e^2N}{\mu\epsilon_0(\omega_{TO}^2} \\ \epsilon_{latt}(\infty) &= 1 + \chi = \epsilon_\infty \end{aligned} \tag{1.27}$$

Replacing the above equations in Eq. 1.26:

$$\epsilon_{latt}(\omega) = \epsilon_\infty + \frac{S\omega_{TO}^2}{(\omega_{TO}^2 - \omega^2 - i\Gamma\omega)} \tag{1.28}$$

Where S is the oscillator strength:

$$S = \epsilon_0 - \epsilon_\infty \tag{1.29}$$

We are dealing with 3C- SiC materials which has the following properties:

- $\omega_{TO} = 796.2\ cm^{-1}$
- $\epsilon_0 = 9.72$
- $\epsilon_\infty = 6.52$
- $\Gamma = 0.02\omega_{TO}$

The fig. 1.3 and 1.4 show the theoretical dielectric function of crystal SiC:

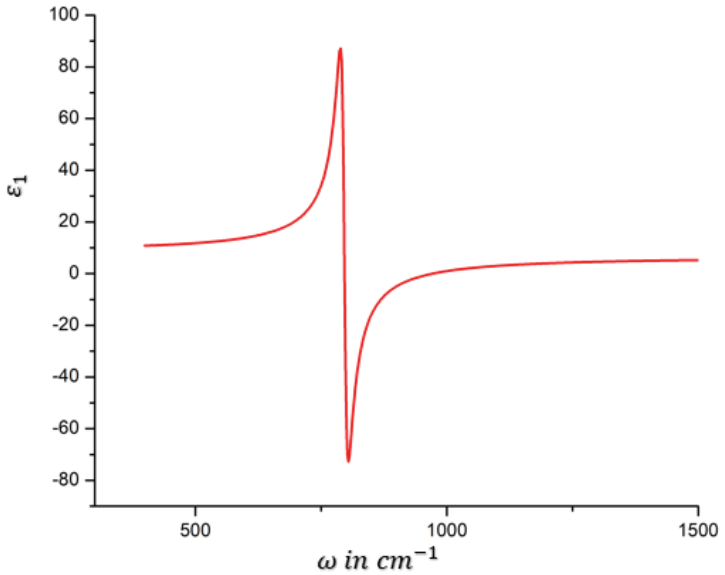

Figure 1.3: The real part of the dielectric function

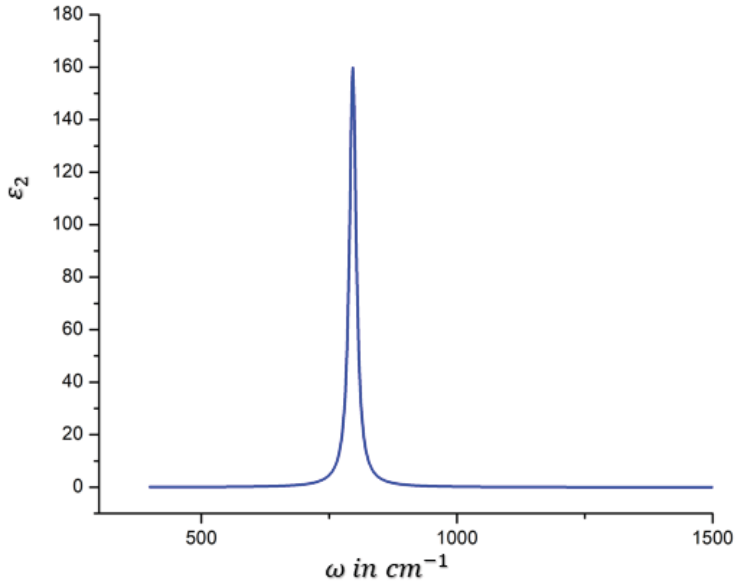

Figure 1.4: The imaginary part of the dielectric function

Chapter 2

Sample Preparations and Characterizations

Lasers are a powerful appliance in many applications, especially in material processing. They are used in many scientific research works and experiments because of their narrow frequency bandwidth, coherence, and high power density. Commonly the light beam is intense enough to vaporize the hardest and most heat resistant materials. Furthermore, because of their high precision, reliability, and spatial resolution, they are widespread in the material processing industry. Laser ablation is the process of removing material from a solid surface by irradiating it with a pulsed laser beam. The process is divided into two regimes:

- Low laser flux, where the material is heated by the absorbed laser energy till it evaporates or sublimates

- High laser flux, the material is typically converted to a plasma

Generally, poly-component materials can be removed and deposited onto substrates to form stoichiometric thin films. This Procedure is called Pulsed Laser Deposition.

Pulsed- Laser Deposition history is tightly attached to the history and development of lasers, which begins at the turn of the 50s and 60s. In the mid-60s, sufficiently powerful pulsed lasers existed already, but limited experiments without important scientific attention were performed to ablate solids and deposit layers. A major breakthrough came in the early 80s when Dijkkamp et al [9] successfully deposited, via an excimer laser a thin film of $YBa_2Cu_3O_7$, a superconducting material, which was of better quality compared to that of films deposited with alternative deposition methods.

2.1 Pulsed-Laser Deposition: Basics and Mechanisms

Over the previous 20 years, PLD has been considered as one of the simplest and most flexible methods for the deposition of thin films. The fig. 2.1 represents a schematic diagram for a typical PLD experimental setup.

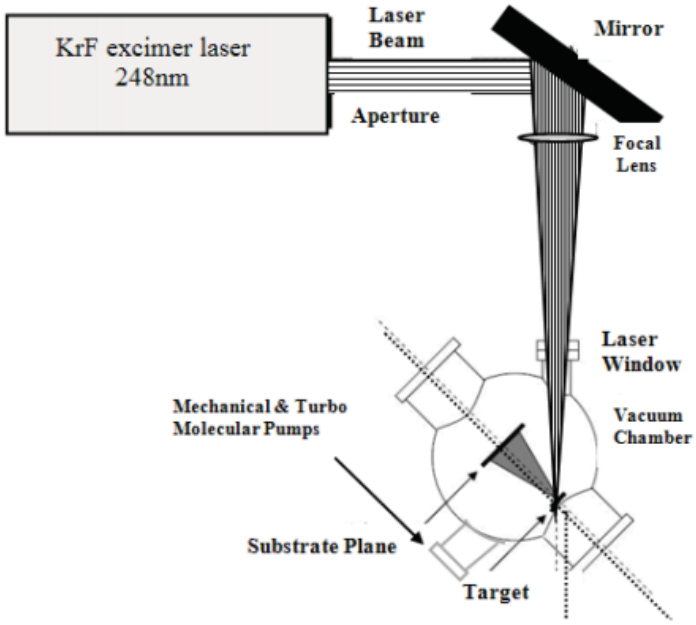

Figure 2.1: Schematic diagram of experimental setup in PLD

Even though PLD is know for its flexibility and conceptual simplicity, the sample growth using this technique is a complex process that can be divided into the following three phases: Light-material interaction, Expansion and Plasma formation, and Film growth.

2.1.1 Synthesis of SiC using PLD

The former record on the PLD of SiC dates back to 1990 [3] [7]. Balooch et al. [3] informed the growth of polycrystalline β-SiC films on Si via an excimer laser. The study focused on obtaining the chemical composition and surface morphology of the films but was restricted to deposition at a substrate temperature of 800 degrees. In the same year, Chen and Murray [7] stated that temperatures of 500 degrees and higher are essential to induce SiC film growth using an Nd:YAG laser.

The SiC deposition was efficiently accomplished using PLD at room temperature in 1994 [4]. In that work, the usage of a KrF excimer, as opposed to Nd:YAG,

was shown to boost the establishment of SiC bonds in the films through the generation of highly energetic species in the plume [5]. After performing transmission electron microscopy (TEM) on the obtained samples, they figured out that the samples were amorphous but contained some crystallites of β-SiC.

Most of the following published studies on the PLD of SiC concentrated on the characterization of crystalline films obtained at temperatures surpassing 700 degrees using several kinds of excimer laser. Mostly, a polycrystalline cubic phase, 3C-SiC, is acquired at 800 degrees and above [30] [20]. Yet Wang et al [26] have indicated a single crystal 4H-SiC formed at 850 degrees.

El Khakani and fellow workers [11] were the former to carry out a methodical research of the growth of SiC films at temperatures below 600 degrees. As deposition temperature is increased, amorphous SiC films with high hardness and elastic modulus were obtained.

In this work, we are interested in growing amorphous and crystal SiC thin film.

2.1.2 Experimental Setup of PLD Deposition

The Pulsed Laser Deposition (PLD) system in this work is represented in the fig. 2.2:

Figure 2.2: PLD system

The main parts of this system are: a high-vacuum chamber supported by a pumping system, an excimer laser, a substrate holder and a target manipulator. The laser is a pulsed LAMBDA PHYSIK KrF excimer having a 248 nm wavelength, a 20 ns pulse duration, and repetition frequency 25Hz. The pulsed excimer laser beam is guided to the target through a line containing two UV mirrors and a 45 cm focal length focusing lens. The focused beam penetrates the high vacuum chamber through a UV transparent window to impinge at an angle of 45^o on the target. By a simple modification in the mirrors orientation and the lens-target distance, one can improve the alignment and fix the focusing of the laser beam.

The pumping unit relies on a Pfeiffer turbomolecular pump and a backing diaphragm pump. The background pressure in the chamber is less than $5 \times 10^{-7} mbar$, as measured by a Pirani gauge.

The substrate manipulator is equipped with a a heater and a water-cooled system thus providing the heating of the substrate to a maximum temperature of 1000 degrees, as measured by a thermocouple located behind the back side of the wafer. The substrate holder whose height can be adjusted can rotate at a desired speed. In our work the target-substrate distance was fixed at about 5 cm, and the substrate was not rotating. Below the substrate holder positions the target manipulator that can hold up to four different targets. To ensure homogeneous target consumption, the target rotates and concurrently moves forward or backward in a toggling motion. The non-rotating substrate consisted of single crystal Si(100) situated 5 cm away parallel to the target. All silicon wafers were chemically cleaned by dipping them consecutively in:

- Acetone at 55 degrees for 10 minutes
- Methanol at 55 degrees for 10 minutes
- 10 % HF acid for 20 seconds
- Deionized water for 2 minutes
- Methanol at room temperature for 5 seconds

The substrate is then dried by nitrogen gas for two minutes, and then it is placed on the substrate holder which should be cleaned by sand paper and then by isopropanol. To prevent contamination, the stainless steel chamber should be cleaned using kimwipes in addition to ethanol. Then, let it dry for 30 minutes with the chamber door open at 30 degrees. The cleaned substrates were then placed inside the chamber which is then pumped down before proceeding with the deposition. The rotating SiC ceramic target should be cleaned by running the laser for few minutes. The chamber pressure was maintained at vacuum level of 7×10^{-7}. During the process, 99.99 % pure argon gas was introduced to the

chamber by lowering chamber pressure to about 5 mTor. The depositions were carried out at Energy = 400 mJ and at different temperatures.

The thickness of each film has been determined using the "DektakXT Stylus Profiler".

The table below shows the conditions used to obtain a SiC thin film.

Sample SiC/Si	Temperature	Thickness	Pressure	Deposition time
A25	25	400 nm	5 mTor	3 hours
A600	600	500 nm	5 mTor	3 hours
A900	900	450 nm	5 mTor	3 hours
V900	900	80 nm	$10^{-6} vacuum$	1 hour
V700	700	50 nm	$10^{-6} vacuum$	1 hour

Table 2.1: Samples synthesized using Pulsed Laser Deposition

2.2 Raman Spectroscopy

Spectroscopy is the study of light-matter interaction as a function of wavelength (λ). Nonetheless, one can define spectroscopy as the use of the absorption, emission, or scattering of electromagnetic radiation by matter to investigate physical processes or to qualitatively or quantitatively analyze the matter, which can be atoms, molecules, atomic or molecular ions, or solids. Redirection of the radiation and/or transitions between the energy levels of the atoms or molecules are results of light-matter interactions. Over many years, Raman Spectroscopy (RS) is considered a spectroscopic technique for quantitative analysis of molecular materials of all types since it is a non-contact characterization procedure that does not necessitate any sample preparation.

In 1928, Sir Chandrasekhra Venkata Raman figured out the phenomenon that bears his name [22]. He used sunlight as the source and a telescope as the collector; the detector was his eyes. That such a feeble phenomenon as the Raman scattering was detected and was indeed remarkable.

Gradually, improvements in the several constituents of Raman instrumentation took place. Primary studies were concentrated on the development of better excitation sources. Progress occurred in the detection systems for Raman measurements as well as developments in the optical train of Raman instrumentation. These developments in Raman instrumentation brought commercial Raman instruments to the present state of the art of Raman measurements. Raman spectroscopy experienced a renaissance in the 1960's when the lasers were invented and started to be used as light sources in spectroscopy.

2.3 The Raman phenomenon

2.3.1 Vibrational Spectroscopy

The vibrations of a poly-atomic molecule can be treated as a system of oscillators. 3N degrees of freedom is the total number of motion for all the nuclear masses in N atomic nuclei molecule [23]. It is a common knowledge that both infrared and Raman spectroscopy fit into vibrational spectroscopy. Any change in the electric dipole moment of the molecule produces a normal mode called infrared-active. Alternatively, a vibrational mode is said to be Raman-active, if the polarizability of the molecule is modified. Thus, strong IR bands are referenced to polar functional groups while non-polar functional groups generates strong Raman bands.

2.3.2 Theoretical Aspects

When light impinges upon a molecule and interacts with the electron cloud and the bonds of that molecule, the Raman effect takes place. During the sponta-

neous Raman effect, a photon excites the molecule from the ground state to a virtual energy state. The molecule returns to a different rotational or vibrational state after emitting a photon and returning to the ground state. The energy difference between the original state and new the state leads to a shift in the emitted photon's frequency away from the excitation frequency. For a molecule to indicate a Raman effect, deformations in the electron cloud with respect to the vibrational coordinate or any modifications in the molecular polarization potential are required. Raman scattering intensity is established by the amount of the polarizability change. A standard Raman spectrum covers the spectral range of "0 - 3500 cm^{-1}".

2.3.3 Raman scattering phenomenon

The fig.2.3 schematically illustrates the Raman scattering.

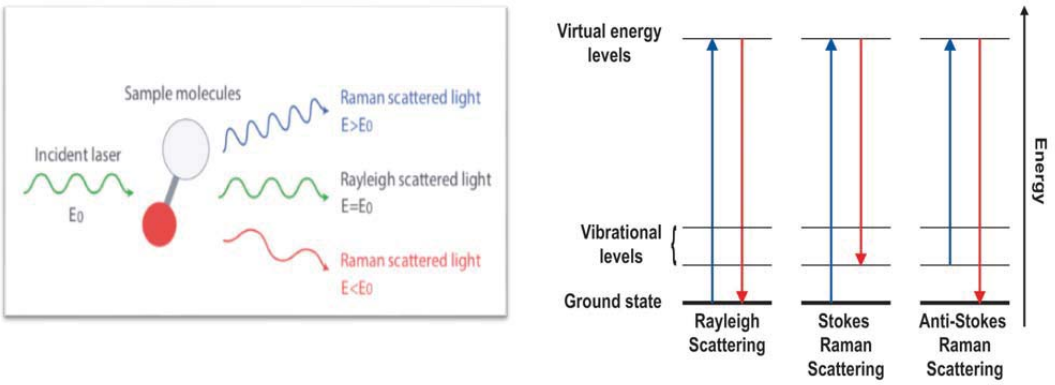

Figure 2.3: Scattering of light by molecules and the Different forms of scattering

Raman spectroscopy special-purpose is to measure the frequency shift of inelastic scattered light from the sample when the photon from incident light hits a molecule and creates a scattered photon [15]. There are two types of scattering: Elastic scattering and Inelastic scattering.

To start with the elastic scattering or Rayleigh scattering where a photon interacts with a molecule, polarizing the electron cloud and raising it to a "virtual" energy state. The molecule will soon (order 10^{-14} sec) fall back down to its ground state, releasing a photon. This release can be in any arbitrary direction, resulting in scattering. However, since the molecule is returning back to its starting state, an equality between the released energy in the photon and the initial photon must occur. Hence the scattered light has the same wavelength as the initial photon. Thus, that Rayleigh scattering carries no information concerning the vibrational energy levels of the sample. On the other hand, during the elastic scattering process photons can lose or gain energy. Accordingly, the

wavelength is respectively increased or decreased. The resulting scattered light can be a photon with a lower frequency than the original photon, this is known as stokes Raman scattering. With higher frequency the scattered light is known as anti-Stokes Raman scattering **figure 1** [1].

The majority of the incident photons are scattered off by the electron cloud without any loss of energy during the light-matter interaction and therefore there is no change in frequency, since the electrons are comparatively light. The scattering is elastic in this case and this is known as Rayleigh Scattering 2.3.The total distribution of the molecules in any energy level is given by the Maxwell-Boltzmann equation:

$$\frac{N_n}{N_m} = \frac{g_n}{g_m} e^{-\frac{(E_n - E_m)}{KT}} \tag{2.1}$$

where:

- $K = 1.3897 \times 10^{-23} JK - 1)$ is the Boltzmann's constant
- T is the given temperature
- N_n is the number of molecules in the excited vibrational energy level n
- N_m is the number of molecules in the ground vibrational energy level m
- $g_{m/n}$ is the degeneracy of the levels in n and m
- $E_n - E_m$ is the energy difference between the vibrational energy levels

As for Raman Scattering, this phenomenon can be understood using the classical theory as follows: The time variation of the electric field (E) of the electromagnetic wave (laser beam) is described as:

$$E(t) = E_0(t) \cos 2\pi\nu_0 t) \tag{2.2}$$

where

- E_0: Vibrational amplitude
- ν_0: Frequency of the laser

When this laser light is incident on a molecule, then an electric dipole moment P is induced:

$$P = \alpha E = \alpha E_0 \cos 2\pi\nu_0 t \tag{2.3}$$

where α is the polarizability of the material which depends on the molecular structure and the nature of the bonds.

If the molecule is vibrating with a frequency ν_m, the physical displacement of the atom about their equilibrium position is expressed as:

$$q = q_0 \cos 2\pi\nu_m t \tag{2.4}$$

where q_0 is the vibrational amplitude.

For a small amplitude of vibration, the polarizability α is a linear function of q and can be approximated using a Taylor series expansion:

$$\alpha = \alpha_0 + (\frac{\partial \alpha}{\partial q})_q q + \cdots \tag{2.5}$$

where

- α_0: is the polarizability at the equilibrium position
- $(\frac{\partial \alpha}{\partial q})_q$: is the rate of change of α with respect to the change in q evaluated at equilibrium position

Combining equations 2.3, 2.4, and 2.5, we obtain:

$$P = \alpha E_0 \cos 2\pi\nu_0 t$$

$$P = \alpha_0 E_0 \cos 2\pi\nu_0 t + (\frac{\partial \alpha}{\partial q})_0 q E_0 \cos 2\pi\nu_0 t$$

$$P = \alpha_0 E_0 \cos 2\pi\nu_0 t + (\frac{\partial \alpha}{\partial q})_0 q_0 E_0 \cos 2\pi\nu_0 t \cos 2\pi\nu_m t$$

$$P = \alpha_0 E_0 \cos 2\pi\nu_0 t + \frac{1}{2}(\frac{\partial \alpha}{\partial q})_0 q_0 E_0 [\cos 2\pi(\nu_0 - \nu_m)t + \cos 2\pi(\nu_0 + \nu_m)t] \tag{2.6}$$

From eqn 2.6, The first term corresponds to an oscillating dipole that radiates light of frequency ν_0 **(Rayleigh Scattering)**. However, the second and third terms represent respectively the Raman Scattering of frequency $\nu_0 - \nu_m$ **(Anti-Stokes)** and of frequency $\nu_0 + \nu_m$ **(Stokes)**.

Note that if $(\frac{\partial \alpha}{\partial q})_0 \approx 0$, then the vibration is not Raman-active.

Ordinarily, Raman Spectroscopy is built on the shift in the energy of the outgoing photon measurements. The chemical composition of the molecules accountable for scattering plays an important role in the wavelength shift of the scattered light. The intensity of Raman scattering is proportional to the magnitude of the change in the molecular polarization.

2.3.4 Instrumentation

A Raman spectrometer is composed of a spectrograph with the following main constituent: an excitation source, a light detector and a light collection and delivery system. The excitation source consists of a laser, while a Charged Coupled Device (CCD) camera is used for detection, and an optical microscope for light collection. A laser of a suitable power, wavelength and stability illuminates the sample. These lasers are generally compendious, fairly vigorous and reliable. The

exciting laser is guided to the sample via a traditional optical system of mirrors and lenses which focus the exciting light onto or into the sample and collects the resulting Raman scattered light. A delicate, low noise detector is mandatory to identify the Raman scattered light. Spectral analysis must be performed on the collected data.

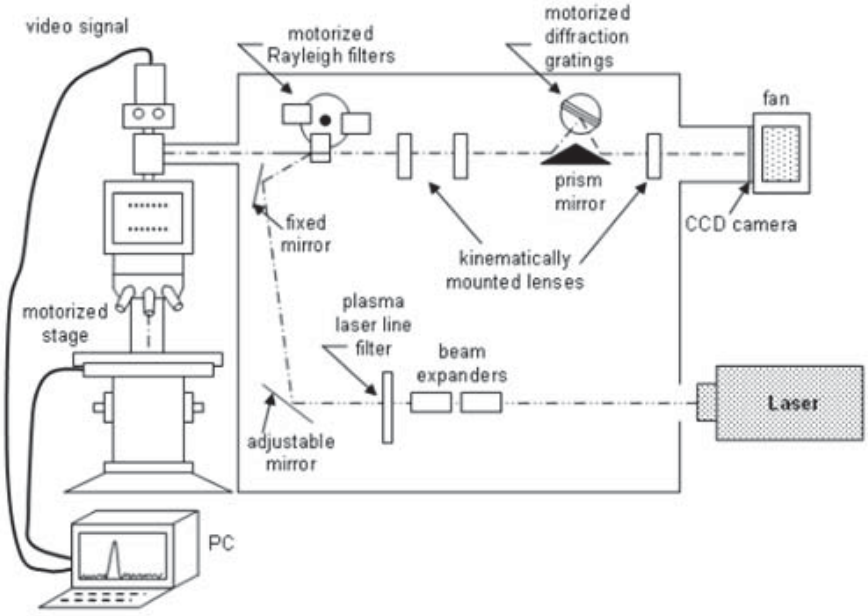

Figure 2.4: Diagram of Raman Microscope System used for Raman spectroscopy and delivery

- Light source: A standard Raman laser consists of several properties, such as a narrow line-width in comparison to the width of the Raman lines in Raman spectrum which is around 1 to 10 cm^{-1}, a low power consumption, a stable power output and a stable wavelength output. Generally speaking, power from the excitation source needed for Raman spectroscopy can range from about 3-10 mWs. Raman spectroscopy requires a monochromatic light source to attain a good spectral resolution. The Raman scattering intensity and the laser power output are independent.

- Light Detector: The system includes a slit, a diffraction grating, a mirror and a detector.

- A CCD camera equipped with a cooling system.

- Rayleigh Filters: They are used to prevent the undesired light that has the the same wavelength as the incident light (Rayleigh or elastic) from reaching the spectrometer and drowning out the relatively weak Raman signal.

- Objective Lenses: The objective lenses not only help in focusing the laser beam but also locating a specific region in a sample, and they are characterized by a certain magnification and a numerical aperture.

2.4 Crystallinity of Samples Using Raman Spectroscopy

Raman Spectroscopy grants the extraction of detailed and specific information on a molecular level that other laser or electronic spectroscopic methods would provide to a limited extent. Of all the various systems that can be investigated by Raman Spectroscopy, we differentiate the following: chemical identity, reactivity, diffusion, charge states, phenomenology at interfaces, crystallinity of samples, in addition to the mechanical and electrical stress and the influence of electric fields on molecular properties

Silicon carbide (SiC) is an auspicious wide band gap semiconductor for high-power, high frequency and high temperature devices, due to its breakdown field, high electron saturated drift velocity and good thermal conductivity. SiC has a massive number of polytypes. The widespread ones are 4H, 6H known as the hexagonal (α-SiC) types, and cubic (3C-SiC) type. Distinct stacking in the SiC double layer produces the building units of all polytypes [19]. Raman scattering is a robust tool which is used in determining the polytype structure of SiC likewise for stress and defect analysis.

The Raman scattering measurements were executed at room temperature in the back-scattering configuration. A laser of wavelength $\lambda = 532nm$ with a 400mW maximum power was used.

The fig. 2.5 and 2.6 show Raman spectra in the 400- 1600 cm^{-1} region for the SiC samples which were deposited using PLD at different temperature.

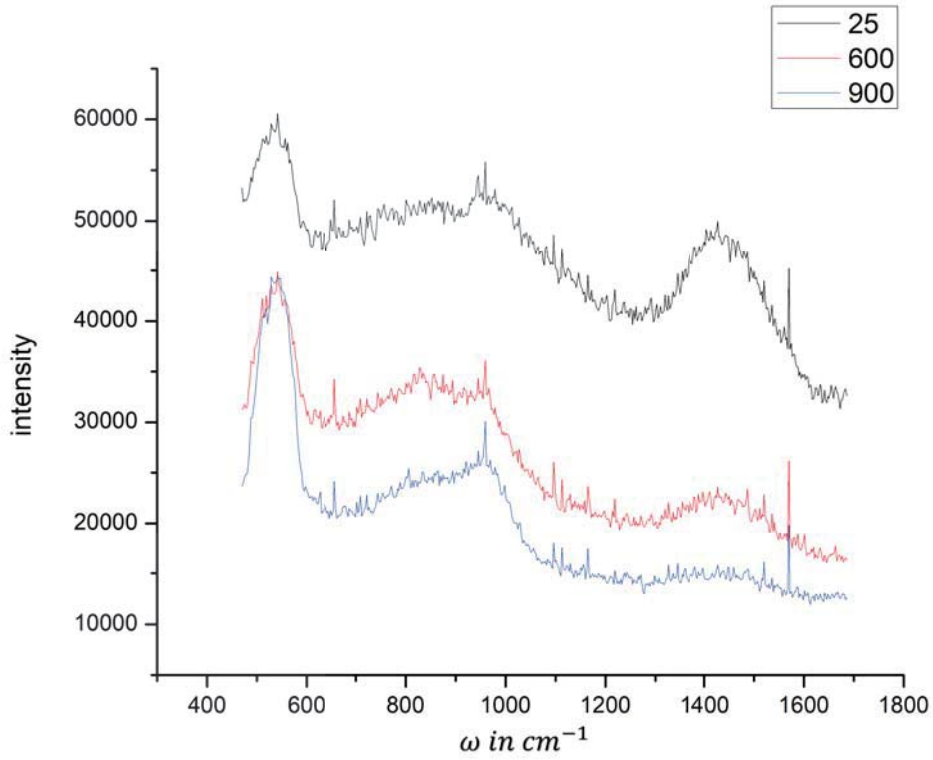

Figure 2.5: Raman spectra of SiC layer grown at different temperature on Si substrate

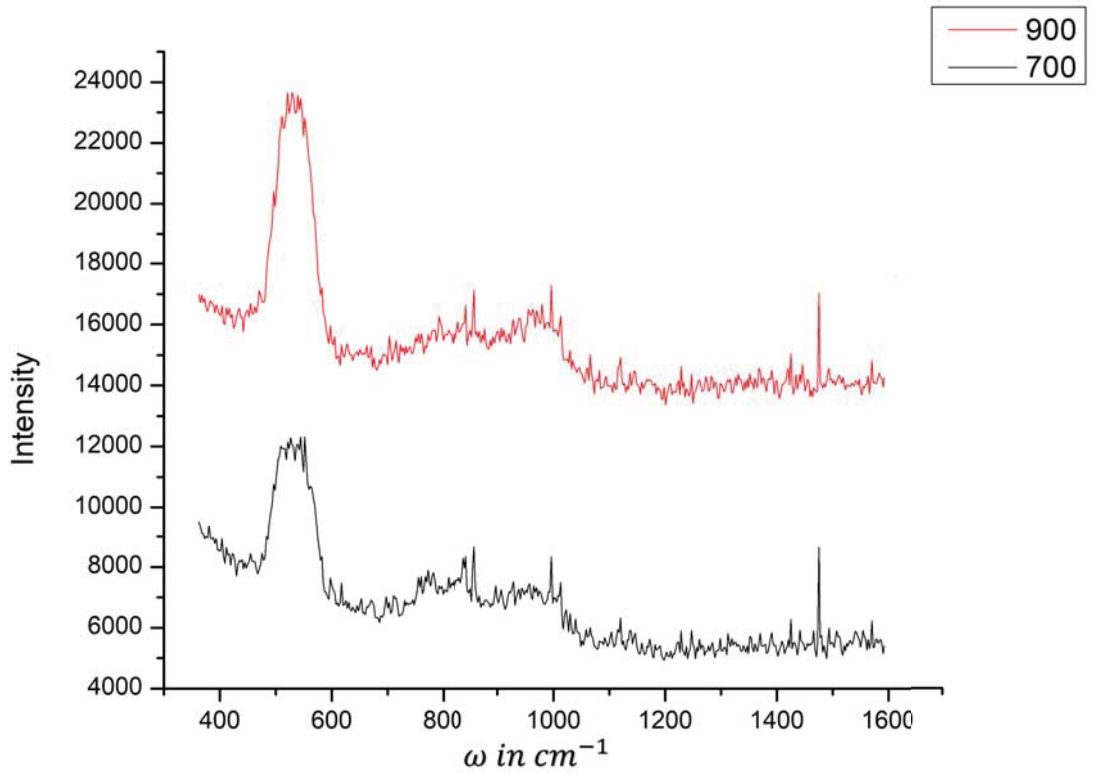

Figure 2.6: Raman spectra of SiC layer grown at different temperature on Si substrate at vacuum pressure

Basically, there are two actual broad bands in the regions of [300-600] and [1300-1600] cm^{-1}. The Raman band of amorphous silicon is represented in [300-600] cm^{-1} band which is attributable to a Raman band related to Si-Si bonds. The other band [1300-1600] cm^{-1} corresponds to that of another amorphous bonds. The [600-1000] cm^{-1} region is connected to Si–C bond because the location of the infrared absorption band due to Si-C bond is at 720 cm^{-1} [27] or 760 cm^{-1} [6]. A very sharp peak corresponds to crystal SiC in the [600-1000] cm^{-1} region. However, in our case the peak is very broad, so our materials are amorphous materials and do not possess a crystalline nature. In addition, as presented in fig. 2.4, as temperature increases the bands occurring in the [1300-1600] cm^{-1} region vanish. However, increasing the temperature did not improve the crystallinity of our material since the band in [600-1000] cm^{-1} region is still broad. On the other hand, in fig 2.5, the [1300-1600] cm^{-1} band does not exist and we still have amorphous SiC. Thus, crystallinity of our samples is not affected by either changing the temperature or by changing the pressure.

Chapter 3

Characterization Method Using FT-IR Spectroscopy

3.1 Basics and Mechanism

3.1.1 Infrared Spectroscopy

IR spectroscopy (which is short for infrared spectroscopy) deals with the infrared region of the electromagnetic spectrum i.e. light having a longer wavelength and a lower frequency than visible light. IR spectroscopy monitors the interaction of infrared radiation and matter. The analysis of this interaction can be examined by measuring absorption, emission, transmission, and reflection. *In our work, we will deal with reflection measurements.*

The baseline in infrared absorption is the transition of a molecule from a ground state (M) to a vibrationally excited state (M*) by absorption of an infrared photon with energy equal to the difference between the energies of the ground and the excited states. On the other hand, infrared emission occurs when a molecule in the excited state (M*) emits a photon during the transition to a ground state (M). Thus, one extracts information by first measuring the frequencies of absorbed infrared photons molecule and then by comprehending these frequencies in terms of the characteristic vibrational motions of the molecule. In complex molecules, some of the frequencies are partnered with functional groups that have characteristic localized modes of vibration.

In infrared spectroscopy analysis, infrared radiation is transmitted through a sample. Part of the infrared light is absorbed by the sample, and the other is reflected by the sample. The final signal at the detector is a spectrum symbolizing a molecular "*fingerprint*" of the given sample. No two molecular structures can have the same infrared spectrum because each composition is a unique combination of atoms. Therefore, infrared spectroscopy can result in a positive **identification** (qualitative analysis) of different kinds of materials.

3.1.2 Fourier Transform Infrared Spectroscopy

A typical laboratory instrument that uses the IR spectroscopy is the Fourier Transform Infrared Spectroscopy **(FT-IR)**. The term Fourier Transform originates from the fact that a Fourier Transform (a mathematical technique) is required to process the raw data into a spectrum to be analyzed. It uses an infrared beam that, after interacting with the sample, provides extremely informative molecular information. The fundamental concept of this method is to measure infrared absorption at characteristic resonance frequencies of the material. In fact, infrared absorption occurs only for molecules with a dipole moment that interacts with the infrared radiation electric field, and when the frequency of the radiation matches the proper frequency of the molecular vibration. Thus, each material possesses its own absorbance spectrum.

Hooke's law explains the vibrations of the molecular bonds. In this approximation, two atoms including the connecting bond are considered as a simple harmonic oscillator where the spring's vibration frequency is connected to the reduced mass $\mu = \frac{m_1 m_2}{m_1+m_2}$ of the two atoms producing the molecule and the spring constant k by the following equation:

$$\tilde{\nu} = \frac{1}{2\pi}\sqrt{\frac{k}{\mu}}$$

The infrared energy region of the electromagnetic spectrum includes the typical values of ν_{vib} which are of order $10^{14}s^{-1}$. In accordance with quantum mechanics, vibrational motion is quantized, and the quantum mechanical solution of a harmonic oscillator is given by:

$$E_i = h\nu(n_i + \frac{1}{2})$$

where $n_i = 0, 1, 2, ..$ is the vibrational quantum number.The light-atom interaction is described by quantum theory. Consequently, the absorbed radiation's energy is a multiple number of the difference in energy between the molecular vibrational ground and excited states, $nh\nu$.Accordingly, when the infrared radiation's frequency matches the molecule vibrational frequency, absorption of light appears and leads to an infrared spectrum that is characteristic of the molecular structure.

Moreover, alongside with the significantly increase of modern software algorithms, FT-IR is an irreplaceable tool for quantitative analysis. The two elementary interest of FT-IR spectroscopy over the dispersive methods of infrared spectral analysis contain the use of the interferometer that leads in extremely fast measurements. Most FT-IR measurements are made in a matter of seconds rather than several minutes because all the frequencies are measured simultaneously. Also, the signal-to-noise ratio (SNR) is proportional to the measurement

time and the number of scans. The other advantage is the high resolution gained in FT-IR spectroscopy without using narrow slits though the resolution is enhanced by increasing mirror travel distance. These advantages, and more other, has made FT-IR analysis almost limitless, highly precise and worthwhile.

FT-IR can use different kinds of interferometers such as the Michelson interferometer, lamellar grating interferometer, and Fabry-Perot interferometer. The principle of the FT-IR spectrometer is as follows: First, a signal known as **interferogram** is generated by the interferometer. The interferogram extracted is a record of intensity by the detector as a function of optical path difference of the two beams of the interferometer. By performing Fourier transform of the interferogram, the final spectrum is obtained.

From this, the intensity, which is a function of path difference x transforms as a whole to give the spectrum S, which depends only on the frequency ν. where:

$$S(\nu) = \int_{-\infty}^{+\infty} I(x) e^{i2\pi\nu x} dx = F^{-1}[I(x)] \tag{3.1}$$

which is the inverse Fourier Transform

$$I(x) = \int_{-\infty}^{+\infty} S(\nu) e^{-i2\pi\nu x} d\nu = F[S(\nu)] \tag{3.2}$$

which is the Fourier Transform

Thus, the inverse Fourier transform integral converts the interferogram I(x), which is function of path difference x, to a spectrum S(ν), which is a function of frequency ν. This calculation is carried out using a computer.

3.1.3 Extracting the spectrum from raw data

It is quite challenging to read the raw data collected on a Fourier transform spectrometer. A Fourier transform is then carried out to decode interferogram and extract actual spectrum $I(\nu)$ from it. The following shows how to conduct a Fourier transform to decrypt: The detector collects the intensity which is a function of the path length differences in the interferometer x and wave-number ν:

$$I(x, \nu) = I(\nu)[1 + \cos(2\pi\nu x)] \tag{3.3}$$

Hence, the total intensity measured at a specific optical path length difference (for every data point at a particular optical path-length difference x) is:

$$I(x) = \int_0^{\infty} I(x, \nu) d\nu \tag{3.4}$$

By determining the inverse Fourier transform, we can solve the wanted spectrum in terms of the measured raw data I(x):

$$S(\nu) = 4 \int_0^{\infty} [I(x) - \frac{1}{2} I(x = 0)] \cos(2\pi\nu x dx \tag{3.5}$$

To wrap up, the normal instrumental process, shown in the above figure, is as follows:

- **The Source:** Infrared energy is emitted from the laser source.
- **The Interferometer:** The beam enters the interferometer where "spectral encoding" takes place. The resulting interferogram signal exits the interferometer.
- **The Sample:** The beam enters the sample compartment where it is reflected off the surface of the sample. This is where specific frequencies of energy, which are uniquely characteristic of the sample, are absorbed.
- **The Detector:** The beam finally passes to the detector for final measurement
- **The Computer:** The measured signal is digitized and sent to the computer where the Fourier transformation takes place.

Figure 3.1: Sample analysis process

3.1.4 Experimental Setup:

Most of the available Fourier transform spectrometers make use of Michelson interferometer, which is easy to construct and operate. The advantages of using the Michelson interferometer are its high throughput, multiplexing, and high precision in frequency measurements.

A typical Michelson interferometer consists of two perpendicular mirrors and beamsplitter.

One of the mirrors is stationary, and the other is a movable mirror. The beamsplitter is designed to transmit half of the light and reflect the other half. Eventually, the two reflected and transmitted rays hit the movable and fixed

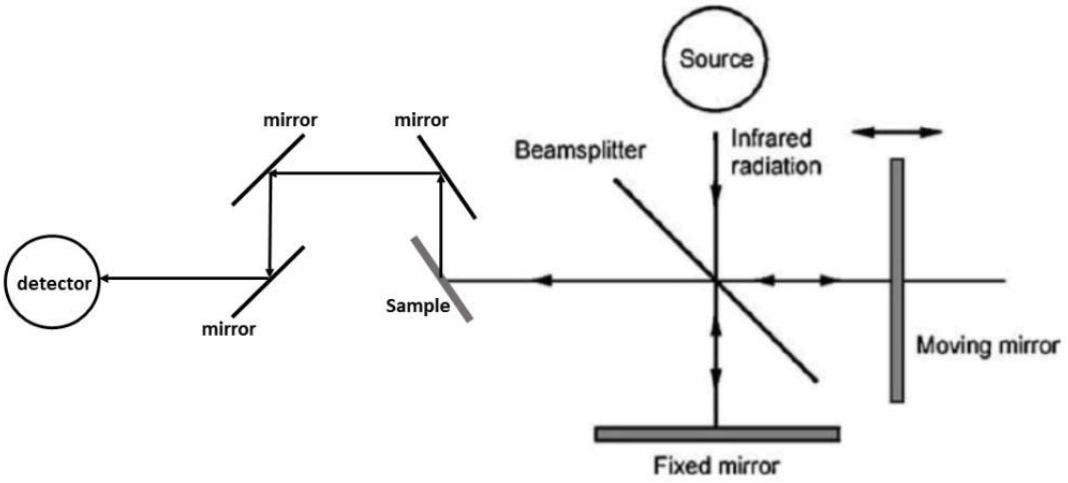

Figure 3.2: Sample analysis process

mirror, respectively. When reflected by the mirrors, the two beams of light recombine at the beamsplitter. Due to the difference in path difference, the two beams interfere with each other resulting in an interference pattern called interferogram. The interferogram has a unique property that every data point, which is a function of the moving mirror position, has information about all of the infrared frequencies generated from the source. This means that as the interferogram is obtained, all frequencies are simultaneously measured.Thus, the use of interferometer facilitates the measurements.

In our work, the used FT-IR system is a Nicolet 4700 spectrometer from Thermo Electron Corporation in the mid-infrared range of 400-4000 cm^{-1}. 100 scans were carried on the samples hile fixing the resolution to cm^{-1} in order to enhance the signal-to-noise ratio. A relative scale for the absorption intensity is needed because the sample compartment is not evacuated. We use a gold coated mirror to collect a background spectrum before each measurement with no sample. The background signal is subtracted from the spectrum of the sample to eliminate the contribution of all of the instrumental and environmental characteristics to the infrared spectrum. As a consequence, all spectral features which exist in the obtained spectrum are rigorously due to the sample. Parameter adjustment and data acquisition carried out by OMNIC software whereas the collected data are plotted and analyzed by the means of Microcal Origin software.

3.1.5 FT-IR Reflectivity Measurements

Unpolarized reflectivity measurements were carried out at room temperature at incident angle $\theta_0 = 45°$ in the mid-infrared frequency range from 400 to 400 cm^{-1} with $1cm^{-1}$ spectral resolution to improve the signal-to-noise ratio of our measurements. The light used is unpolarized. In our experiments, a Nicolet 4700 spectrometer from Thermo Electron Corporation, a KBr beamsplitter, and a DTGS detector were used. To check the validity of our experiment, we measure the reflectivity of our crystal 4H-SiC. We found that the reflectivity measurements are with agreement with the literature [8].

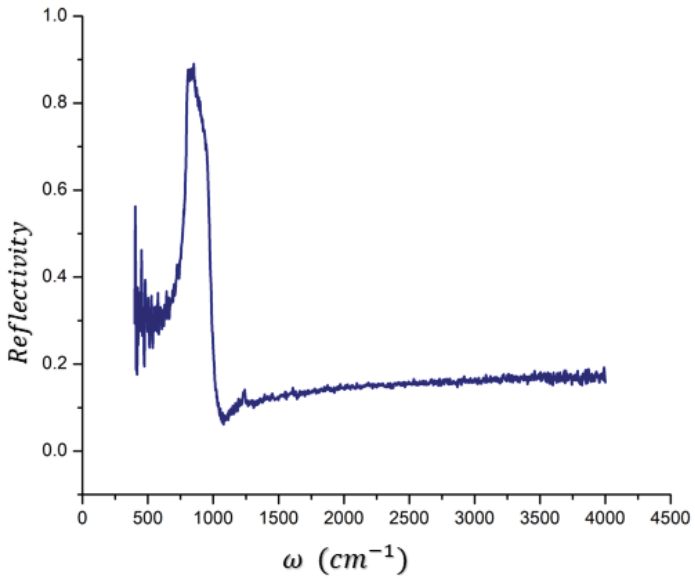

Figure 3.3: Reflectivity measurements of 4H-SiC as function of wavelength

We proceeded to determine the dielectric property of 4H-SiC and compare it to the crystal model presented in chapter 1. The calculations are explained in details in the next chapter.

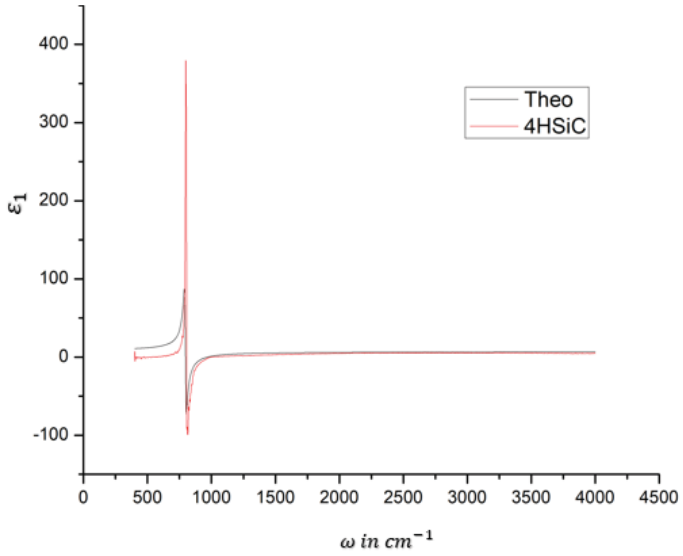

Figure 3.4: Real part of the dielectric function of 4H-SiC and the theoretical model as function of ω

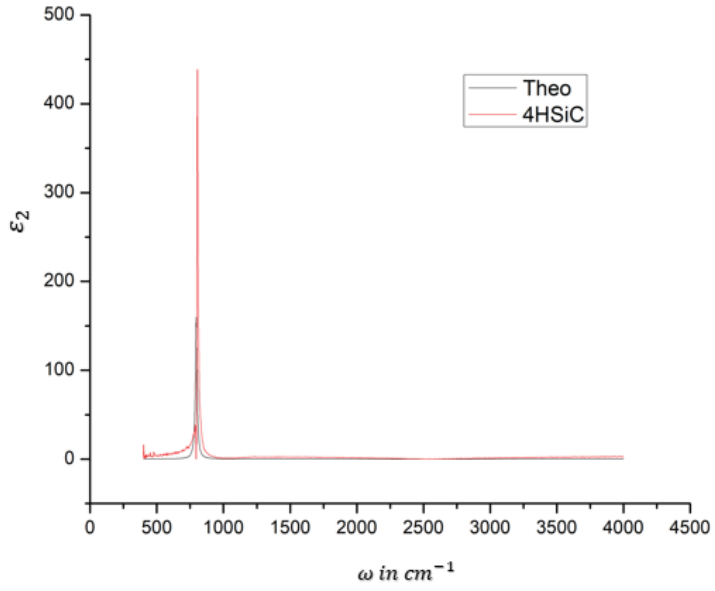

Figure 3.5: Imaginary part of the dielectric function of 4H-SiC and the theoretical model as function of ω

Chapter 4

Multi-layer System

The aim of this work is to determine the dielectric property of any material using reflectivity measurement of unpolarized light. Because the material is not pure crystal, the calculations can not rely on the theoretical model presented in chapter 1. Hence, there is no available model to manipulate the dielectric properties for amorphous materials. To do so, we used the Transfer Matrix Method which has been used to calculate the optical reflectance of multilayer structures by creating a chain of multiplied single layer-transfer matrices, accompanied by the boundary conditions of the electromagnetic fields at the interfaces of the structure. By obtaining the reflectance in a very abstract way, we can estimate the main optical properties of a given combination of films.

4.1 Fresnel Theory

Augustin-Jean Fresnel derived the most fundamental equations in classical optics, ***Fresnel Equations***. Fresnel equations link the relation between the amplitudes, phases and polarization of the reflected and transmitted wave between two materials with different refractive indices, to the incident wave's parameters. Fresnel equations are coherent with the treatment of light in Maxwell's equations. Consequently, the behavior of the electromagnetic waves at the air-semiconductor interface is determined by setting the boundary conditions of Maxwell's equations at each interface. Thus, it is possible to determine the reflectance which is the fraction of light reflected at the interface between two materials. The ratio depends on the angle of incidence of the radiation, so the behavior at the interface depends on the polarization of light.

It is worth mentioning that we have two kind of polarization:

- P-polarized ***(parallel polarization)*** :
  - The electric field is parallel to the plane of incidence

– The magnetic field is perpendicular to the plane of incidence

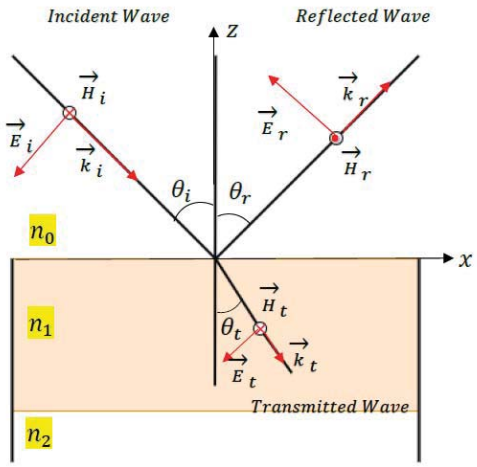

Figure 4.1: Field vectors of the incident, transmitted, and reflected waves in case the electric field vectors lie within the plane of incidence (P polarization)

- s-polarized ***(perpendicular polarization)***
  - The electric field is perpendicular to the plane of incidence
  - The magnetic field is parallel to the plane of incidence

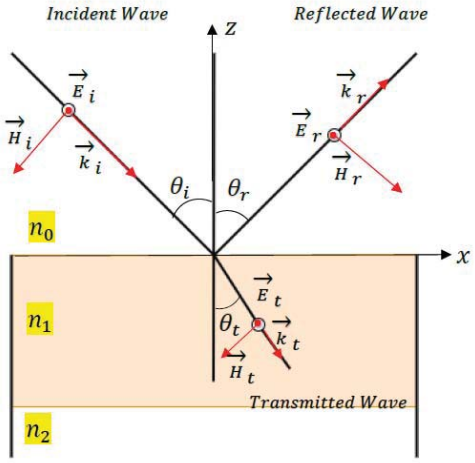

Figure 4.2: Field vectors of the incident, transmitted, and reflected waves in case the electric field vectors lie within the plane of incidence (s polarization)

4.2 Fresnel Equations

To obtain Fresnel coefficients, two optical media with different refractive indices separated by an interface are considered, as shown in figure 1. A plane inc incident optical wave is propagating toward the interface with wave vector $\vec{k_i}$ oriented at an angle θ_i with respect to the interface normal. E_i is the electric field amplitude in the plane of incidence. Upon approaching the interface, the wave will be partially transmitted to medium 2 and partially reflected. The transmitted wave will propagate at angle θ_t which is determined by *Snell's Law:*

$$n_1 \sin\theta_i = n_2 \sin\theta_t \tag{4.1}$$

where n_1 and n_2 are the refractive indices of medium 1 and 2 respectively. According to the law of reflection, the incident angle θ_i is equal to the reflected angle θ_r. E_t and E_r represent respectively the amplitude of the transmitted and reflected electric field. Therefore, to determine the total reflectance, these two amplitudes should be obtained.

To achieve this, the boundary conditions for the electric and magnetic fields at an interface between two media with different electromagnetic properties should be applied. The boundary conditions for the tangential components of **E** and **H** are extracted by applying Faraday's and Ampere's laws to a rectangular loop straddling the surface, whereas the boundary conditions for the normal components for **D** and **B** are derived from operating Gauss's and Coulomb's laws to a circular cylinder extending from one material to the other. In our case we are interested in the tangential boundary condition which is: the tangential component (tangent to the surface) of the electric field $\vec{E_i}$ and the magnetic field $\vec{H_i}$ should be continuous across the boundary.

In other words, the boundary condition for the electric field is:

$$E_i \cos\theta_i + E_r \cos\theta_r = E_t \cos\theta_t \tag{4.2}$$

Whereas, the boundary condition for the magnetic field, which is collinear in all three waves, becomes:

$$H_i - H_r = H_t \tag{4.3}$$

Since the electromagnetic wave is transverse, the incident field crossing the interface can be decomposed into two polarization component, P-polarization and S-polarization. In the following section, Fresnel equations will be derived for both cases, p- and s- polarization.

4.2.1 Fresnel Equations for P-polarization

First, the P-polarization case in figure 1 is considered. Due to symmetry, the reflected and transmitted waves are of the same polarization.

To determine the solution of these two equations, we should recall the relation between the electric and magnetic field amplitudes for each wave. Maxwell's equation states that these amplitudes in any plane electromagnetic wave must satisfy:

$$H = \sqrt{\frac{\epsilon}{\mu}} E \tag{4.4}$$

where ϵ and μ are the electric permittivity and the magnetic permeability, respectively, of the material in which the wave propagates.*At optical frequency* μ *= 1.*

Because the refractive index is given by $n = \sqrt{\epsilon}$, we have:

$$\begin{aligned} H_{i,r} &= n_1 E_i \\ H_t &= n_2 E_t \end{aligned} \tag{4.5}$$

Thus from equation 3, we have:

$$n_1(E_i - E_r) = n_2 E_t \tag{4.6}$$

Linking equation 2 and 6, we obtain **Fresnel Equations for P-polarization**:

$$\begin{aligned} r_p &= \frac{n_1 \cos\theta_t - n_2 \cos\theta_i}{n_1 \cos\theta_t + n_2 \cos\theta_i} \\ t_p &= \frac{2 n_1 \cos\theta_i}{n_1 \cos\theta_t + n_2 \cos\theta_i} \end{aligned} \tag{4.7}$$

Here, we can define the reflection and transmission coefficients:

$$\begin{aligned} r &= \frac{E_r}{E_i} \\ t &= \frac{E_t}{E_i} \end{aligned} \tag{4.8}$$

4.2.2 Fresnel Equations for S-polarization

Similarly, for the case of s-polarization (figure 2), the boundary conditions are:

$$E_i + E_r = E_t \tag{4.9}$$

$$-H_i \cos\theta_i + H_r \cos\theta_i = H_t \cos\theta_t \tag{4.10}$$

In which, Fresnel equations for s-polarization are:

$$r_s = \frac{n_1 \cos\theta_i - n_2 \cos\theta_2}{n_1 \cos\theta_i + n_2 \cos\theta_2}$$
$$t_s = \frac{2n_1 \cos\theta_i}{n_1 \cos\theta_i - n_2 \cos\theta_2} \tag{4.11}$$

4.3 Transfer Matrix Method

The reflection of light from a single interface between two optical media is described by ***Fresnel Equations***, explained in section 1. However, when there are several interfaces, the reflections themselves might also be partially reflected or transmitted, as shown in the below figure. According to the exact optical path length, constructive and destructive interference can occur from these reflections. The total reflection of the system is the sum of infinite number of reflections.

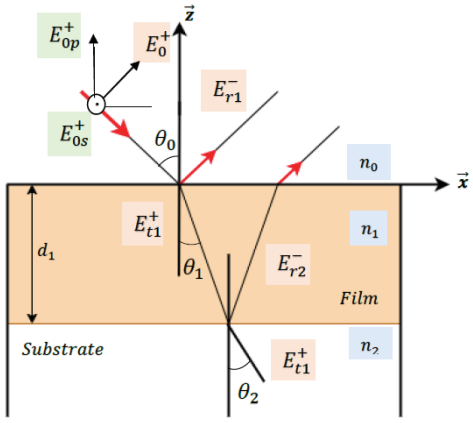

Figure 4.3: Reflection and Transmission at interfaces

In this manner, **Transfer matrix-method TMM** is a powerful mathematical tool in the analysis of light propagation through layered dielectric media and in solving Maxwell's equations in complex media [28]. The central idea lies that electric and magnetic fields at two different positions are linked together through a transfer matrix. As a result, the coherent optical reflectance of a multi-layered structure are represented as a product of matrices.

TMM relies on the boundary continuity conditions of the electric field implied by Maxwell's equations, which offer all the physical background of the electric and magnetic fields of the waves to be connected across the boundaries of two different materials and manipulated at the material's interface. This method make use of simple matrix operations that connects the top and bottom fields of a single layer. The final expression for the reflectance of multi-layer structure is calculated through two steps:

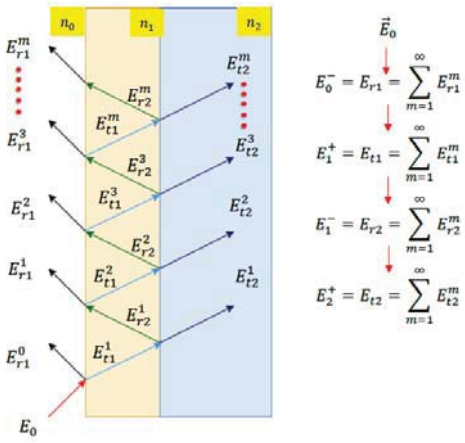

Figure 4.4: Single-layer film on substrate

- First: Calculating the characteristic matrix, which includes Fresnel reflection coefficient, for each layer.
- Second: The reflectance is derived from the matrices product of individual layers.

4.3.1 Transfer Matrix for a single layer-film on a substrate

By setting up Maxwell's equations and applying the correct boundary conditions, Transfer Matrix method can model the reflectance and transmittance of light propagating a medium.

In order to determine the reflectance for a single layer-film on a substrate using TMM, we first consider, according to the below figure:.

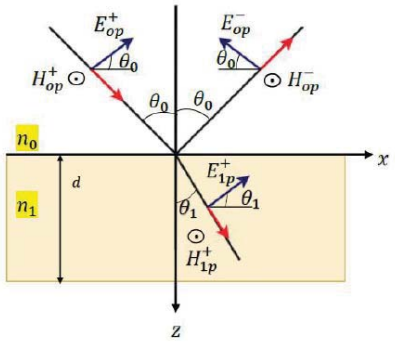

Figure 4.5: Field vectors of incident, reflected and transmitted waves in p-polarization

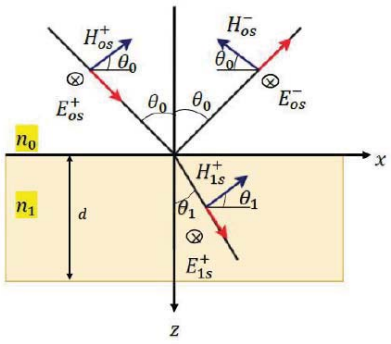

Figure 4.6: Field vectors of incident, reflected and transmitted waves in s-polarization

We examine a plane wave incident at $z = 0$, the plane of incidence being the plane xOz, the angle of reflection θ_0 and the refraction angle θ_1. Besides,we consider an interface between two dielectric media of refractive indices n_0 and n_1. We also donate the amplitudes of the electric vectors approaching the surface by E_{0p}^{+}, E_{0s}^{+}. Whereas, the reflected wave presented as E_{0p}^{-}, E_{0s}^{-} and the transmitted wave by E_{1p}^{+}, E_{1s}^{+}.

Generally speaking, the electric and magnetic plane wave solutions of Maxwell's equation at a fixed angular frequency take the form:

$$E(r,t) = E_0 e^{i(wt \pm \mathbf{k}.\mathbf{r})}$$

$$H(r,t) = H_0 e^{i(wt \pm \mathbf{k}.\mathbf{r})}$$

where the sign of the dot product of $\mathbf{k}$ and r, $\mathbf{k}.r$, depends on the wave propagation direction.

A phase factor must be included for the electric vector of incident, reflected, and transmitted waves at the interfaces between medium n_0 and medium n_1.

The phases will take the following forms:

$$e^{i(wt - \frac{2\pi n_0 \sin\theta_0 x}{\lambda} - \frac{2\pi n_0 \cos\theta_0 z}{\lambda})} \text{ (incident)}$$

$$e^{i(wt - \frac{2\pi n_0 \sin\theta_0 x}{\lambda} + \frac{2\pi n_0 \cos\theta_0 z}{\lambda})} \text{ (reflected)}$$

$$e^{i(wt - \frac{2\pi n_1 \sin\theta_1 x}{\lambda} - \frac{2\pi n_1 \cos\theta_1 z}{\lambda})} \text{ (transmitted)}$$

It is noteworthy that in a sinusoidal steady state, Maxwell's equations can be expressed in terms ofa phasor which is a complex number representing a sinusoidal function whose amplitude $\mathbf{A}$, angular frequency ω, and initial phase ϕ are time-invariant. Thus, for the above notation of electric and magnetic fields as function

of space and time in a frequency domain, the phasor form of Maxwell's equations is written as follows:

$$\begin{aligned} \nabla \times \mathbf{E} &= -i\omega\mu\mathbf{H} \\ \nabla \times \mathbf{H} &= i\omega\epsilon\mathbf{E} + \sigma\mathbf{E} \\ \nabla \cdot \mathbf{E} &= 0 \\ \nabla \cdot \mathbf{H} &= 0 \end{aligned} \tag{4.12}$$

Where the electric and magnetic field phasors depend on space coordinates only, ϵ is the dielectric permittivity, and μ is the magnetic permeability which is set to be 1.

Applying the curl operator to the electric plane wave solution and comparing to the first equation in the above set of equations, the relation between **H** and **E** is:

$$\begin{aligned} \mathbf{H} &= \sqrt{\frac{\epsilon}{\mu}}\mathbf{K} \times \mathbf{E} \\ \mathbf{H} &= \sqrt{\epsilon}\mathbf{K} \times \mathbf{E} \\ \mathbf{H} &= n\mathbf{K} \times \mathbf{E} \end{aligned} \tag{4.13}$$

where $\sqrt{\epsilon} = n$ and the tangential components of the electric field E and the magnetic field H represents the x and y components of the fields. They are given in the first medium as:

$$\begin{aligned} E_{0x} &= (E_{0p}^{+}e^{-ix_0z} + E_{0p}^{-}e^{+ix_0z})\cos\theta_0 \\ E_{0y} &= (E_{0p}^{+}e^{-ix_0z} + E_{0p}^{-}e^{+ix_0z}) \\ H_{0x} &= (-E_{0s}^{+}e^{-ix_0z} + E_{0s}^{-}e^{+ix_0z})n_0\cos\theta_0 \\ H_{0y} &= (E_{0p}^{+}e^{-ix_0z} - E_{0p}^{-}e^{+ix_0z})n_0 \end{aligned} \tag{4.14}$$

And in the second medium:

$$\begin{aligned} E_{1x} &= E_{1p}^{+}e^{-ix_1z}\cos\theta_1 \\ E_{1y} &= E_{1s}^{+}e^{-ix_1z} \\ H_{1x} &= -n_1E_{1s}^{+}e^{-ix_1z}\cos\theta_1 \\ H_{1y} &= n_1E_{1p}^{+}e^{-ix_1z} \end{aligned} \tag{4.15}$$

where $x_i = \frac{2\pi n_i \cos\theta_i}{\lambda}$

Hence, to determine the reflection and transmission of the electromagnetic waves through a medium, the continuity relation, provided below, of the tangential field boundary condition, derived from Maxwell's equations, should be applied. The boundary conditions are:

$$\begin{aligned} E_{0t} &= E_{1t} \\ H_{1t} - H_{0t} &= J \end{aligned} \tag{4.16}$$

Where

- J is the surface current density which is equals to zero in case of dielectric materials
- subscript t is for the tangential component either x or y

Applying the boundary condition by equating the tangential components of the electric and magnetic fields at $z = 0$, we get:

$$\begin{aligned} E_{0x} &= E_{1x} \implies \\ (E_{0p}^{+} + E_{0p}^{-})\cos\theta_0 &= E_{1p}^{+}\cos\theta_1 \\ E_{0y} &= E_{1y} \implies \\ E_{0p}^{+} + E_{0p}^{-} &= E_{1s}^{+} \\ H_{0x} &= H_{1x} \implies \\ (-E_{0s}^{+} + E_{0s}^{-})n_0\cos\theta_0 &= -n_1 E_{1s}^{+}\cos\theta_1 \\ H_{0y} &= H_{1y} \implies \\ (E_{0p}^{+} - E_{0p}^{-})n_0 &= n_1 E_{1p}^{+} \end{aligned} \tag{4.17}$$

and on the plane $z = d$, we have:

$$\begin{aligned} (E_{1p}^{+}e^{-ix_1d} + E_{1p}^{-}e^{+ix_1d})\cos\theta_1 &= E_{2p}^{+}e^{-ix_2d}\cos\theta_2 \\ E_{1p}^{+}e^{-ix_1d} + E_{1p}^{-}e^{+ix_1d} &= E_{2s}^{+}e^{-ix_2d} \\ (-E_{1s}^{+}e^{-ix_1d} + E_{1s}^{-}e^{+ix_1d})n_1\cos\theta_1 &= -n_2 E_{2s}^{+}e^{-ix_2d}\cos\theta_2 \\ (E_{1p}^{+}e^{-ix_1d} - E_{1p}^{-}e^{+ix_1d})n_1 &= n_2 E_{2p}^{+}e^{-ix_2d} \end{aligned} \tag{4.18}$$

Generalizing the problem by considering the interface between i^{th} and $(i+1)^{th}$ layers, so the electric and magnetic fields should satisfy the following conditions:

$$\begin{aligned} E_i^{+} + E_i^{-} &= E_{i+1}^{+} + E_{i+1}^{-} \\ H_i^{+} - Hi^{-} &= H_{i+1}^{+} - H_{i+1}^{-} \end{aligned} \tag{4.19}$$

Where each electric and magnetic field is composed of a p-polarized component and s-polarized one.

Therefore, at non-normal incidence the Fresnel coefficients associated with the interface between two media (i and i+1) are given by the below equations (Knowing that the definitions of $r = \frac{E_{i-1}^{-}}{E_{i-1}^{+}}$ and $t = \frac{E_i^{+}}{E_{i-1}^{+}}$):

$$\begin{aligned} r_{i\perp} &= \frac{\tilde{n_{i-1}}\cos\theta_{i-1} - \tilde{n_i}\cos\theta_i}{\tilde{n_{i-1}}\cos\theta_{i-1} + \tilde{n_i}\cos\theta_i} \\ r_{i\parallel} &= \frac{\tilde{n_i}\cos\theta_{i-1} - \tilde{n_{i-1}}\cos\theta_i}{\tilde{n_i}\cos\theta_{i-1} + \tilde{n_{i-1}}\cos\theta_i} \\ t_{i\perp} &= \frac{2\tilde{n_{i-1}}\cos\theta_{i-1}}{\tilde{n_{i-1}}\cos\theta_{i-1} + \tilde{n_i}\cos\theta_i} \\ t_{i\parallel} &= \frac{2\tilde{n_{i-1}}\cos\theta_{i-1}}{\tilde{n_i}\cos\theta_{i-1} + \tilde{n_{i-1}}\cos\theta_i} \end{aligned} \tag{4.20}$$

Also, the total reflectance for the p-polarized and s-polarized are:

$$\begin{aligned} R_{i\perp} &= r_{i\perp} r_{i\perp} * \\ R_{i\parallel} &= r_{i\parallel} r_{i\parallel} * \end{aligned} \tag{4.21}$$

To reach the matrix form, equations 17 and 18 should be changed to:

$$\begin{aligned} E_{i-1}^{+} &= \frac{(e^{i\delta_{i-1}} E_i^{+} + r_i e^{i\delta_{i-1}} E_i^{-})}{t_i} \\ E_{i-1}^{-} &= \frac{(r_i e^{-i\delta_{i-1}} E_i^{+} + e^{-i\delta_{i-1}} E_i^{-})}{t_i} \end{aligned} \tag{4.22}$$

Where i represent the two interfaces, $i = 1$ for the first interface (air-thin film) and $n = 2$ for the second interface (thin film-substrate), and $\delta_i = \frac{2\pi n_i d_i \cos\theta_i}{\lambda}$ stands for the phase change of the beam while propagating inside the film.

Any system of equations can be outlined using a matrix form:

$$\begin{bmatrix} E_{i-1}^{+} \\ E_{i-1}^{-} \end{bmatrix} = \frac{1}{t_i} \begin{bmatrix} e^{i\delta i-1} & r_i e^{i\delta i-1} \\ r_i e^{-i\delta i-1} & e^{-i\delta i-1} \end{bmatrix} \begin{bmatrix} E_i^{+} \\ E_i^{-} \end{bmatrix} \tag{4.23}$$

where the characteristic matrix of a single layer:

$$C_i = \begin{bmatrix} e^{i\delta i-1} & r_i e^{i\delta i-1} \\ r_i e^{-i\delta i-1} & e^{-i\delta i-1} \end{bmatrix} \tag{4.24}$$

For a single film, the reflectance (R) and the transmittance (T) are given by:

$$\begin{aligned} R &= \frac{(E_0^{-})(E_0^{-})^*}{(E_0^{+})(E_0^{+})^*} \\ T &= \frac{(E_2^{+})(E_2^{+})^*}{(E_0^{+})(E_0^{+})^*} \end{aligned} \tag{4.25}$$

Hence, to determine these coefficients, we should consider the matrices for i=1 and i=2: For i=1, eqn 4.23 will be:

$$\begin{bmatrix} E_0^{+} \\ E_0^{-} \end{bmatrix} = \frac{1}{t_1} \begin{bmatrix} e^{i\delta 0} & r_1 e^{i\delta 0} \\ r_1 e^{-i\delta 0} & e^{-i\delta 0} \end{bmatrix} \begin{bmatrix} E_1^{+} \\ E_1^{-} \end{bmatrix} \tag{4.26}$$

For i=2:

$$\begin{bmatrix} E_1^{+} \\ E_1^{-} \end{bmatrix} = \frac{1}{t_2} \begin{bmatrix} e^{i\delta 1} & r_2 e^{i\delta 1} \\ r_2 e^{-i\delta 1} & e^{-i\delta 1} \end{bmatrix} \begin{bmatrix} E_2^{+} \\ E_2^{-} \end{bmatrix} \tag{4.27}$$

Combining the two above, we get the relation between the incident and transmitted beams:

$$\begin{bmatrix} E_0^{+} \\ E_0^{-} \end{bmatrix} = \frac{1}{t_1 t_2} \begin{bmatrix} 1 & r_1 \\ r_1 & 1 \end{bmatrix} \begin{bmatrix} e^{i\delta_1} & r_2 e^{i\delta_1} \\ r_2 e^{-i\delta_1} & e^{-i\delta_1} \end{bmatrix} \begin{bmatrix} E_2^{+} \\ E_2^{-} \end{bmatrix} \tag{4.28}$$

Expressing the matrix product

$$(C_1)(C_2) = \begin{bmatrix} a & b \\ c & d \end{bmatrix} \tag{4.29}$$

where a, b , c , and d can be calculated using the matrix multiplication rules.

Therefore, the reflectance and the transmittance can be formulated as:

$$\begin{aligned} R &= \frac{cc^*}{aa^*} \\ T &= \frac{(t_1 t_2)(t_1^* t_2^*)}{aa^*} \end{aligned} \tag{4.30}$$

4.3.2 Transfer Matrix for a multi-layer thin film

Now, let us elaborate the transfer matrix method for a single layer to a multi-layer system.

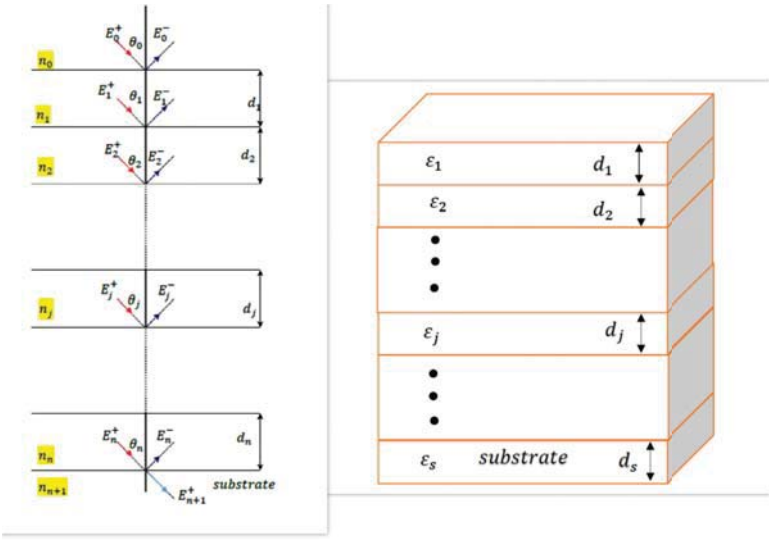

Figure 4.7: The reflectance and transmission though a multi-layer semiconductor

As shown in the figure above, we consider a stack of parallel-plane layers of indices: *1,2,..,j,..,n-1* which are placed between the ambient layer (0) and the substrate (n).

n_j and d_j are,respectively , the refractive index and the geometrical thickness for the layer j. Snell's law relates the angle θ_j to θ_{j+1}:

$$n_j \sin\theta_j = n_{j+1} \sin\theta_{j+1} \tag{4.31}$$

.

Thus, to extract the total response of the given structure we should determine the total reflectance for the structure i.e the ratio of $E_0^+ and E_0^-$.

The transfer matrix method will provide the linear relation between $E_0^+, E_0^-, E_{n+1}^+, E_{n+1}^-$ by performing a characteristic matrix multiplication over the layers. The expression for the whole multi-layer structure is elaborated as:

$$\begin{bmatrix} E_0^+ \\ E_0^- \end{bmatrix} = \frac{(C_1)(C_2)\cdots(C_{n+1})}{t_1 t_2 \cdots t_{n+1}} \begin{bmatrix} E_{n+1}^+ \\ E_{n+1}^- \end{bmatrix} \tag{4.32}$$

with

$$(C_M) = \begin{bmatrix} e^{i\delta_{m-1}} & r_m e^{i\delta_{m-1}} \\ r_m e^{-i\delta_{m-1}} & e^{-i\delta_{m-1}} \end{bmatrix} \tag{4.33}$$

and

$$(C_1)(C_2)\cdots(C_{n+1}) = \begin{bmatrix} a & b \\ c & d \end{bmatrix} \tag{4.34}$$

Concluding that the reflectance and transmittance are:

$$\begin{aligned} R &= \frac{(E_0^-)(E_0^-)*}{(E_0^+)(E_0^+)*} = \frac{cc*}{aa*} \\ T &= \frac{(t_1 t_2 \cdots t_{n+1})(t_1 * t_2 * \cdots t_{n+1}*)}{aa*} \end{aligned} \tag{4.35}$$

We have applied the transfer matrix method for a 3 layers system (air - thin film of SiC - silicon). A notation for the matrix elements is introduced which will enable expressions relating to finite number of layers. First, we will consider an unpolarized light where there is no difference between the perpendicular and parallel polarizations. We donate by $\tilde{n_{j-1}} = n_{j-1} + ik_{j-1}$ the complex refractive index of layer j-1 and $\tilde{n_j} = n_j + ik_j$ for layer j. The complex Fresnel's coefficients between layers j-1 and j are given as: $r_j = g_j + ih_j$ and $t_j = 1 + r_j = 1 + g_j + ih_j$

Thus

$$\begin{aligned} g_j &= real(r_j) \\ h_j &= imag(r_j) \end{aligned} \tag{4.36}$$

Moreover, the phase shift of the $(j-1)^{th}$ layer is written as:

$$\begin{aligned} e^{i\delta_{j-1}} &= e^{i2\pi\omega d_{j-1}\cos\theta_{j-1}(n_{j-1}+i*k_{j-1})} \\ exp^{i\delta_{j-1}} &= e^{\alpha_{j-1}} * e^{i\gamma_{j-1}} \end{aligned} \tag{4.37}$$

where: $\alpha_{j-1} = -2\pi\omega k_{j-1} d_{j-1}\cos\theta_{j-1}$ and $\gamma_{j-1} = i2\pi\omega n_{j-1} d_{j-1}\cos\theta_{j-1}$

Point out that all the components of single matrices are complex, so the j^{th} matrix is given as:

$$(C_j) = \begin{bmatrix} e^{i\delta_{j-1}} & r_j e^{i\delta_{j-1}} \\ r_j e^{-i\delta_{j-1}} & e^{-i\delta_{j-1}} \end{bmatrix} = \begin{bmatrix} p_j + iq_j & r_j + is_j \\ t_j + iu_j & v_j + iw_j \end{bmatrix} \tag{4.38}$$

By applying simple mathematics, we extract the new defined coefficients as follows:

$$\begin{aligned}
p_j &= e^{\alpha_{j-1}} \cos\gamma_{j-1} \\
q_j &= e^{\alpha_{j-1}} \sin\gamma_{j-1} \\
r_j &= e^{\alpha_{j-1}} (g_j \cos\gamma_{j-1} - h_j \sin\gamma_{j-1}) \\
s_j &= e^{\alpha_{j-1}} (h_j \cos\gamma_{j-1} + g_j \sin\gamma_{j-1}) \\
t_j &= e^{-\alpha_{j-1}} (g_j \cos\gamma_{j-1} + h_j \sin\gamma_{j-1}) \\
u_j &= e^{-\alpha_{j-1}} (h_j \cos\gamma_{j-1} - g_j \sin\gamma_{j-1}) \\
v_j &= e^{-\alpha_{j-1}} \cos\gamma_{j-1} \\
w_j &= -e^{-\alpha_{j-1}} \sin\gamma_{j-1}
\end{aligned} \tag{4.39}$$

For calculating the reflectance for multilayer structure of n layers, one should simplify the characteristic matrix product of the individual layer matrices. The recurrence relations allow the elements of product matrices to be expressed in a double suffix way as:

$$(C_1)(C_2)\cdots(C_{n+1}) = \begin{bmatrix} p_{1,n+1} + iq_{1,n+1} & r_{1,n+1} + is_{1,n+1} \\ t_{1,n+1} + iu1, n+1 & v_{1,n+1} + iw_{1,n+1} \end{bmatrix} \tag{4.40}$$

Where the recurrence relations are determined as:

$$\begin{aligned}
p_{1,n+1} &= p_{1n}p_{n+1} - q_{1n}q_{n+1} + r_{1n}t_{n+1} - s_{1n}u_{n+1} \\
q_{1,n+1} &= q_{1n}p_{n+1} + p_{1n}q_{n+1} + s_{1n}t_{n+1} + r_{1n}u_{n+1} \\
r_{1,n+1} &= p_{1n}r_{n+1} - q_{1n}s_{n+1} + r_{1n}v_{n+1} - s_{1n}w_{n+1} \\
s_{1,n+1} &= q_{1n}r_{n+1} + p_{1n}s_{n+1} + s_{1n}v_{n+1} + r_{1n}w_{n+1} \\
t_{1,n+1} &= t_{1n}p_{n+1} - u_{1n}q_{n+1} + v_{1n}t_{n+1} - w_{1n}u_{n+1} \\
u_{1,n+1} &= u_{1n}p_{n+1} + t_{1n}q_{n+1} + w_{1n}t_{n+1} + v_{1n}u_{n+1} \\
v_{1,n+1} &= t_{1n}r_{n+1} - u_{1n}s_{n+1} + v_{1n}v_{n+1} - w_{1n}w_{n+1} \\
w_{1,n+1} &= u_{1n}r_{n+1} + t_{1n}s_{n+1} + w_{1n}v_{n+1} + v_{1n}w_{n+1}
\end{aligned} \tag{4.41}$$

Eventually, the reflectance will have the following term:

$$R = \frac{cc*}{aa*} = \frac{t_{1,n+1}^2 + u_{1,n+1}^2}{p_{1,n+1}^2 + q_{1,n+1}^2} \tag{4.42}$$

In our model, we followed the same strategy derived above but for unpolarized light. Consequently, the recurrence relations should be calculated for both the perpendicular (s) and parallel (p) polarizations.

$$\begin{aligned}
R_s &= \frac{t_{12s}^2 + u_{12s}^2}{p_{12s}^2 + q_{12s}^2} \\
R_p &= \frac{t_{12p}^2 + u_{12p}^2}{p_{12p}^2 + q_{12p}^2}
\end{aligned} \tag{4.43}$$

The total reflectivity of the system is:

$$R = \frac{1}{2}(R_p + R_s) \tag{4.44}$$

At the same time, the effective Fresnel coefficients are provided as:

$$\begin{aligned} r_p &= \frac{r_{1p} + r_{2p}e^{-2i\delta}}{1 + r_{1p}r_{2p}e^{-2i\delta}} \\ r_s &= \frac{r_{1s} + r_{2s}e^{-2i\delta}}{1 + r_{1s}r_{2s}e^{-2i\delta}} \\ r &= \frac{1}{2}(r_p + r_s) \end{aligned} \tag{4.45}$$

To obtain the total phase, one should write r as:

$$\begin{aligned} r &= \sqrt{R}e^{i}\phi \\ \ln r &= \ln\sqrt{R} + i\phi \end{aligned} \tag{4.46}$$

In this manner, $\phi = imag(\ln r)$

4.4 Kramers-Kronig Analysis

The primary goal is to link the only extracted experimental data, the reflectance $\mathbf{R}(\omega)$, to the real and imaginary parts of the optical dielectric function.

Kramers-Kronig relations are named in honor of Hans Kramers and Ralph Kronig. They are bidirectional mathematical relations, linking the real and imaginary parts of complex numbers i.e the real and imaginary parts are dependent, so the real part can be determined from the imaginary part (or vice versa)..

A function, $\chi(s) = \chi_1(s) + i\chi_2(s)$, should have the following properties in order to satisfy Kramers Kronig Relations:

- The locations of the poles of $\chi(\omega)$ are below the real axis and that the function is analytic in the upper half of the complex plane
- The function $\chi_1(\omega)$ is even and the function $\chi_2(\omega)$ is odd with respect to real w
- $\int \frac{\chi(\omega)}{\omega}$ tends to zero when taken around an infinite semicircle in the upper part of the complex plane

Suppose that $\chi(s) = \chi_1(s) + i\chi_2(s)$ is a complex function, where $\chi_1(s)$ and $\chi_2(s)$ are real numbers. The Kramers-Kronig relations are:

$$\begin{aligned} \chi_1(\omega) &= \frac{P}{\pi}\int_{-\infty}^{\infty}\frac{\chi_2(s)ds}{s-\omega} \\ \chi_2(\omega) &= -\frac{P}{\pi}\int_{-\infty}^{\infty}\frac{\chi_1(s)ds}{s-\omega} \end{aligned} \tag{4.47}$$

where P is the Cauchy principle value.
Manipulating the real part of $\chi(s) = \chi_1(s) + i\chi_2(s)$ and splitting the integral into two parts, we achieve:

$$\begin{aligned} \chi_1(\omega) &= \frac{P}{\pi}\int_{-\infty}^{\infty}\frac{\chi_2(s)ds}{s-\omega} \\ \chi_1(\omega) &= \frac{P}{\pi}[\int_{-\infty}^{0}\frac{\chi_2(p)dp}{p-\omega} + \int_{0}^{\infty}\frac{\chi_2(s)ds}{s-\omega}] \end{aligned} \tag{4.48}$$

From the second property, substitute p for -s and $\chi_2(-s) = -\chi_2(s)$ to get

$$\begin{aligned} \chi_1(\omega) &= \frac{2P}{\pi}\int_{0}^{\infty}\frac{s\chi_2(s)ds}{s^2-\omega^2} \\ \chi_2 1(\omega) &= -\frac{2\omega P}{\pi}\int_{0}^{\infty}\frac{\chi_1(s)ds}{s^2-\omega^2} \end{aligned} \tag{4.49}$$

This analysis (K-K) is one of the principle tools of the investigation of light matter interaction phenomena in all media [16]. It gives constraints for testing the self-consistency of experimental or model-generated data. Also K-K relations allow optical data inversion, i.e. information on dispersive phenomena can be determined by converting measurements of absorptive phenomena over the whole spectrum and vice versa.

In this manner, the reflectivity coefficient $r(\omega)$ is a complex function defined at the surface of a crystal as the light intensity ratio of the reflected and incident beams:

$$r(\omega) = \frac{E_r ef}{E_i nc} = \rho(\omega)e^{i\theta(\omega)} \tag{4.50}$$

where

- $r(\omega)$ is expressed in the polar notation with modulus ρ and argument θ
- $\rho(\omega) = \sqrt{R(\omega)}$ with $R(\omega)$ being the only measured experimental data
- and $\theta(\omega)$ is the phase change between the reflected and transmitted rays which cannot be measured using the experiment

In this manner, Kramers-Kronig analysis of infrared spectra is used to extract the phase change $\theta(\omega)$ from the measured experimental data $R(\omega)$.

In order to achieve our goal in determining the complex dielectric function of the system $\epsilon(\omega) = \epsilon_1(\tilde{\omega}) + i\epsilon_2(\omega)$, the relation between $r(\omega)$ and $n(\tilde{\omega}) = n(\omega) + ik(\omega)$ should be provided:

$$r(\omega) = \frac{\tilde{n_2}\cos\theta_1 - \tilde{n_1}\cos\theta_1}{\tilde{n_2}\cos\theta_1 + \tilde{n_1}\cos\theta_1} = \sqrt{R}e^{i\phi} \tag{4.51}$$

$$\ln r(\omega) = \ln\sqrt{R(\omega)} + i\phi(\omega) \tag{4.52}$$

Using eqn 4.47, we obtain the phase change between the incident and reflected rays as:

$$\begin{aligned}\phi(\omega) &= -\frac{\omega P}{\pi}\int_0^\infty \frac{\ln R(s)ds'}{s'^2-\omega^2} \\ \phi(\omega) &= -\frac{\omega}{\pi}\int_0^\infty \frac{(\ln R(\omega')-\ln R(\omega))d\omega'}{\omega'^2-\omega^2}\end{aligned} \tag{4.53}$$

Performing integration by parts to the above equation, we obtain more suitable expression of $\phi(\omega)$:

$$\phi(\omega) = -\frac{1}{2\pi}\int_0^\infty \ln\frac{|s+\omega|}{|s-\omega|}\frac{d\ln R(s)}{ds}ds \tag{4.54}$$

Eqn 4.54, is the phase shift theoretical form that illustrates whole reflection spectrum from zero to infinite frequencies. Yet, testing the above integral indicates that only a limited part of the whole spectrum contributes remarkably to $\phi(\omega)$. The two ranges that do not contribute in the integral are: the regions where the reflectance is constant, and the regions where $\ln\frac{|s+\omega|}{|s-\omega|}$ is very weak when either $s >> \omega$ or $s << \omega$. Accordingly, the significant contributions come from the range in the vicinity of ω_0, in which $\ln\frac{|s+\omega|}{|s-\omega|}$ is sharply peaked, and from regions where the reflectivity alters expeditiously. In conclusion, for IR study, lattice vibrations are the main reason behind light absorption, so the key involvements to $\phi(\omega)$ are from The Reststrahlen Region and its neighborhoods.

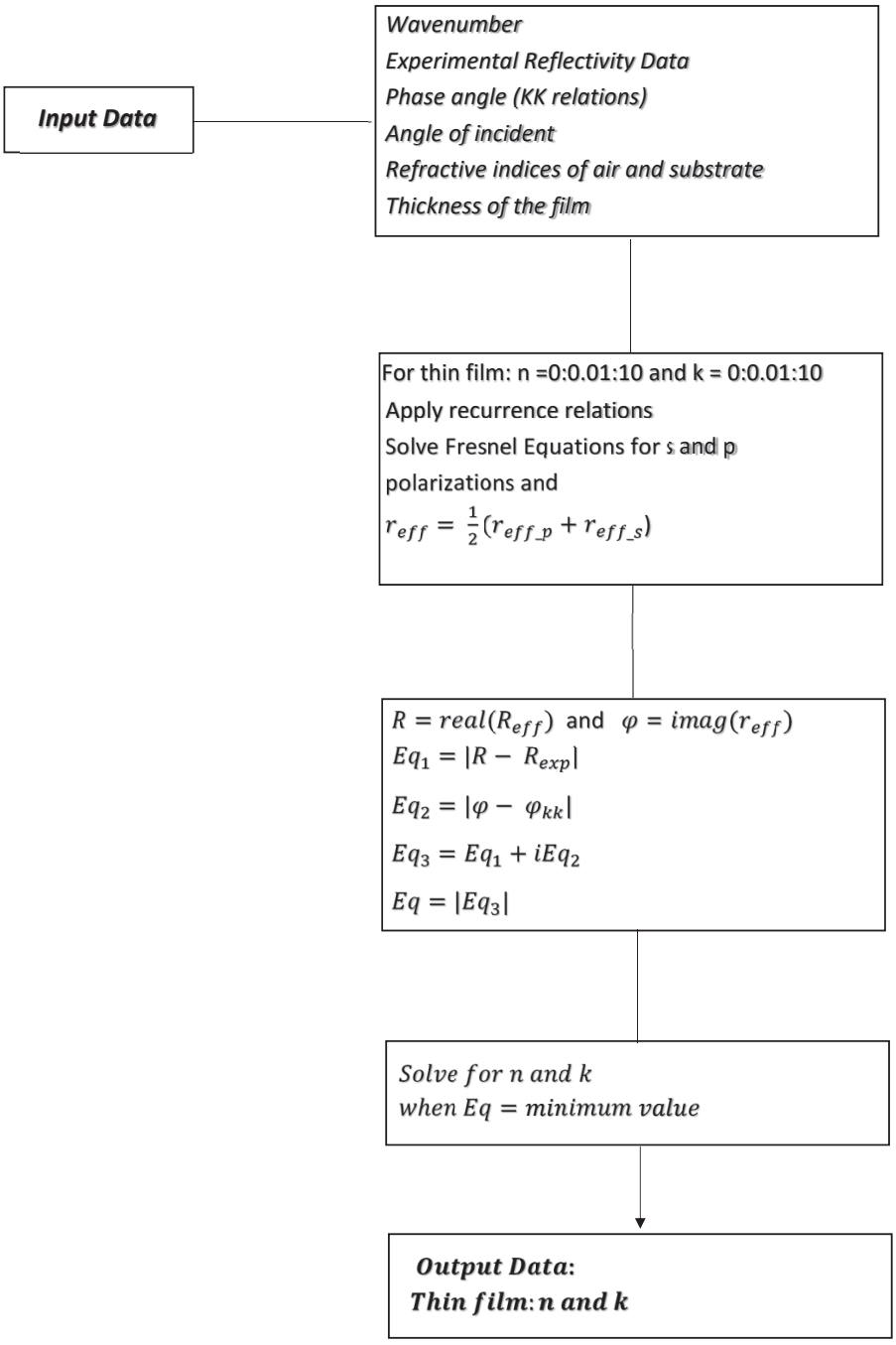

Figure 4.8: MATLAB code Algorithm to calculate the complex refractive index of a thin film

Chapter 5

Results and Discussions

In this chapter, we use the model developed to derive from infrared reflectivity measurements the complex infrared dielectric function of amorphous silicon carbide films grown on silicon.

The amplitudes of the rays reflected from the measured samples were measured using the experimental setup described in chapter 3. The phases of the plane infrared electromagnetic waves were obtained using the Kramers-Kronig conversion theorem. Then, using the numerical technique described in chapter 3, we deduced the complex infrared dielectric function of the amorphous silicon carbide films grown at different temperatures and pressures using the PLD technique.

5.1 Measurements

FT-IR measurements were performed on the samples investigated to measure their reflectivity spectra. Then, Kramers-Kronig theorem was applied on the measured spectra to retrieve the phase shift as a function of the excitation wavelength. From the knowledge of the reflectivity and phase vs the excitation wavelength, we were able to derive the complex refractive index (n +ik) spectrum for each sample. The real and imaginary parts of the dielectric function are then readily derived from the relationships:

$\epsilon_1(\omega) = n^2(\omega) - k^2(\omega)$ and $\epsilon_2(\omega) = 2n(\omega)k(\omega)$.

The fig. 5.1-5.4 show the real "ϵ_1" and imaginary "ϵ_2" of the dielectric function ϵ as function of ω:

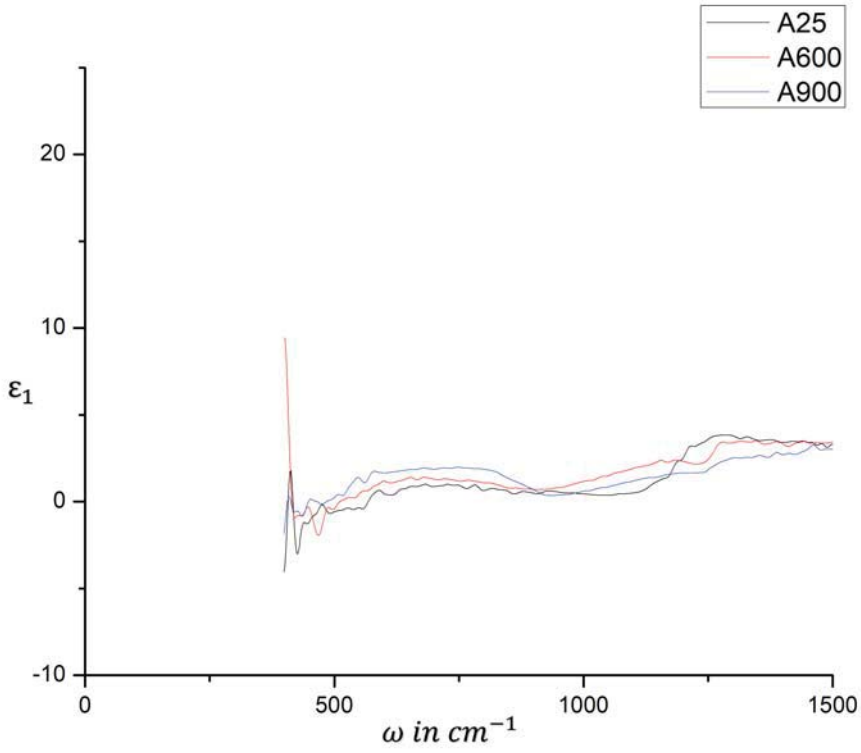

Figure 5.1: Real part of the dielectric function as function of ω for SiC thin film synthesized at 5 mTorr

Fig.5.1 shows that the growth temperature has no effect on the real part of the infrared dielectric function. Furthermore, the real part of all the grown films do not present features related to resonance frequencies. From these results we can conclude that the grown films can be described with the model of Einstein, i.e., with independent oscillator that do not present specific resonance frequencies.

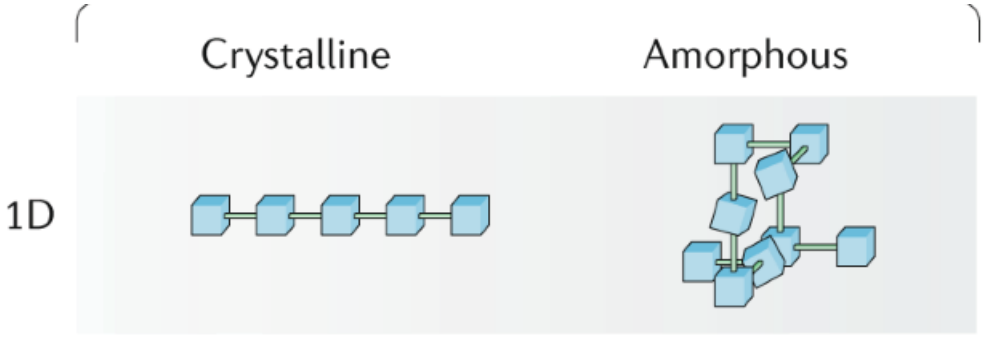

Figure 5.2: 1D Crystal and Amorphous Chain

Hence, all the grown films were amorphous and temperature does not seem to enhance the film crystallinity.

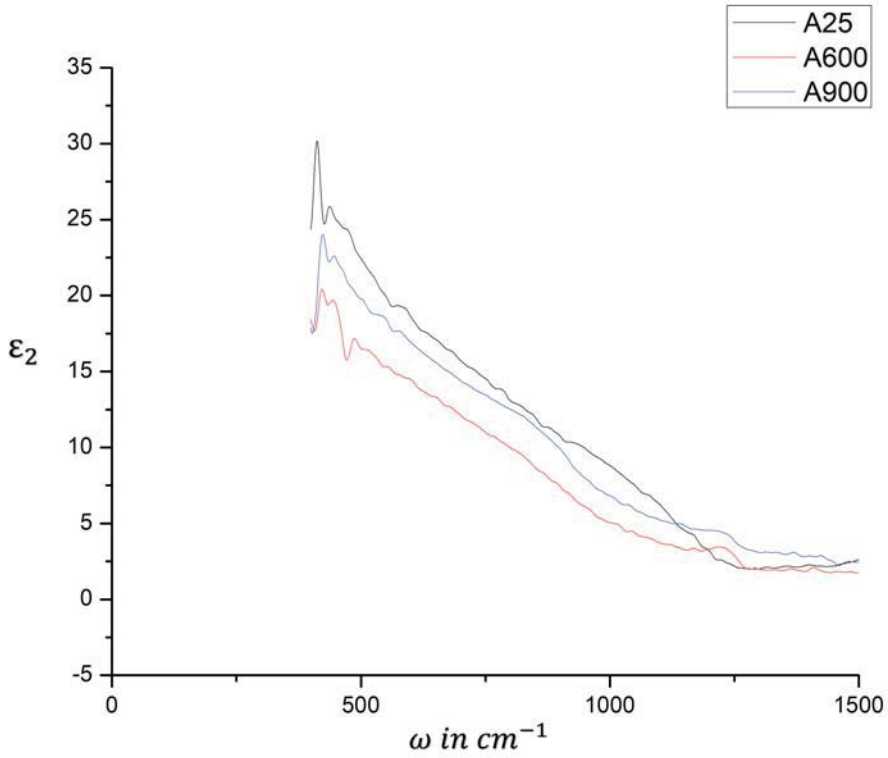

Figure 5.3: Imaginary part of the dielectric function as function of ω for SiC thin film synthesized at 5 mTorr

Fig.5.2 shows that the growth temperature also has no effect on the imaginary part of the infrared dielectric function. Moreover, the imaginary parts are larger than the real parts of the grown films and extend from 500 $cm^{-1}$to 1500 cm^{-1}. The broadness of the imaginary part is related to the features that appear in the corresponding Raman Spectra.

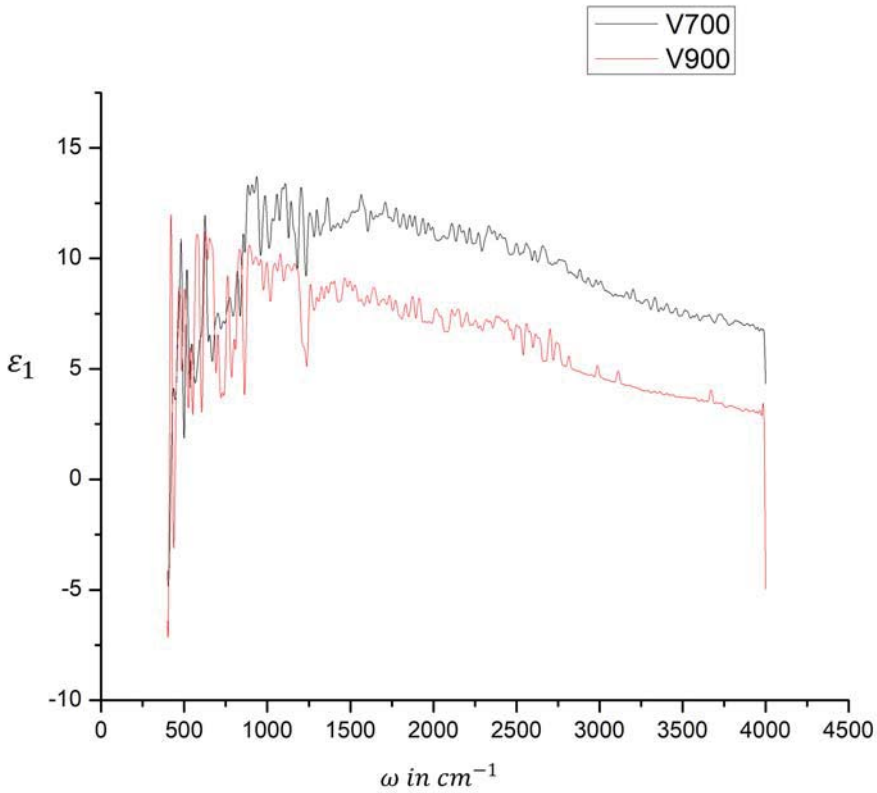

Figure 5.4: Real part of the dielectric function as function of ω for SiC thin film synthesized under vacuum

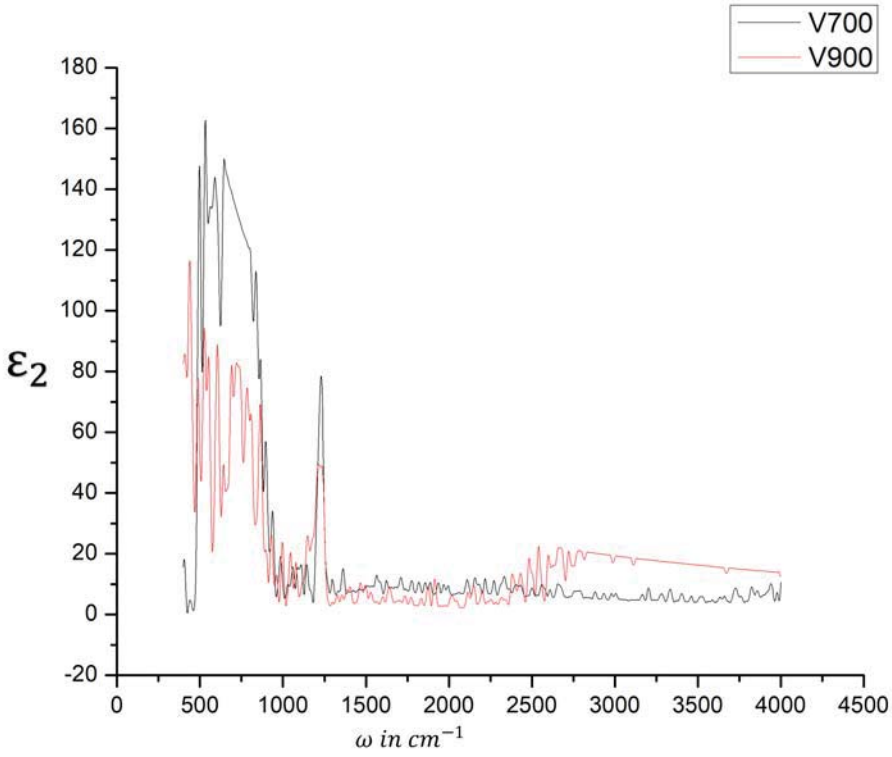

Figure 5.5: Imaginary part of the dielectric function as function of ω for SiC thin film synthesized at vacuum

Fig.5.3 and Fig.4 present the real and imaginary parts of the complex infrared dielectric functions of silicon carbide films grown at a very low pressure (10^{-6} mbar). The film growth with a very low pressure allowed to reduce the imaginary part below the real part of the dielectric function at high frequency. As can be seen from the corresponding Raman spectra, this is due to the fact that the growth at a very low pressure help eliminate bonds whose vibration frequencies lie in the frequency range between 1000 cm^{-1} and 1600 cm^{-1}.

To make sure that the collected data are reasonable, we recalculate the reflectance "R" and the phase shift "ϕ" as function of ω and compare them to the experimental ones.

The fig. 5.6-5.15 show the calculated reflectance R_{cal} and the experimental reflectance data R_{exp} as function of ω. In addition, the calculated phase shift ϕ_{cal} and phase shift determined by Kramers-Kronig equations ϕ_{KK} as function of ω are shown.

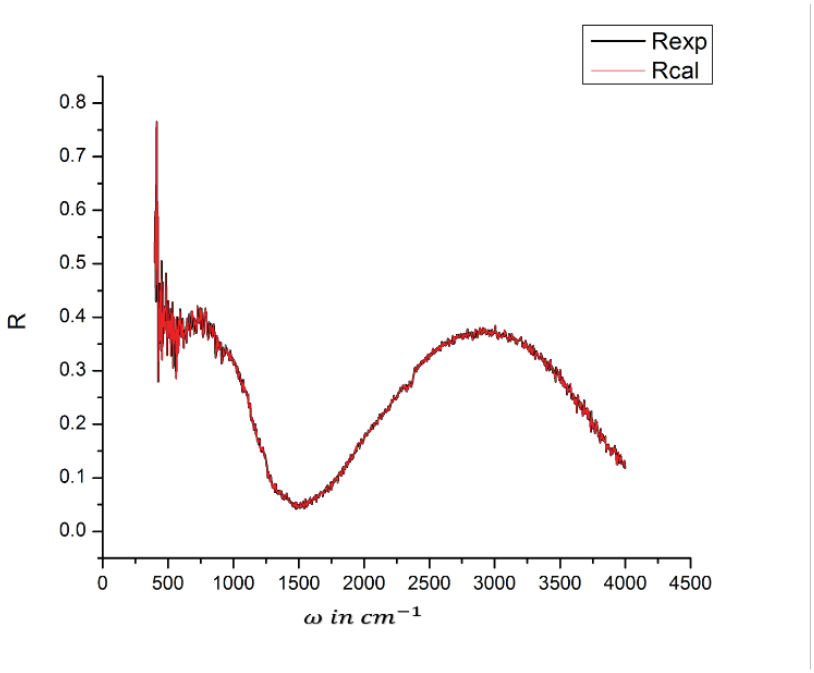

Figure 5.6: Reflectivity of SiC deposited at 25 degree as function of ω

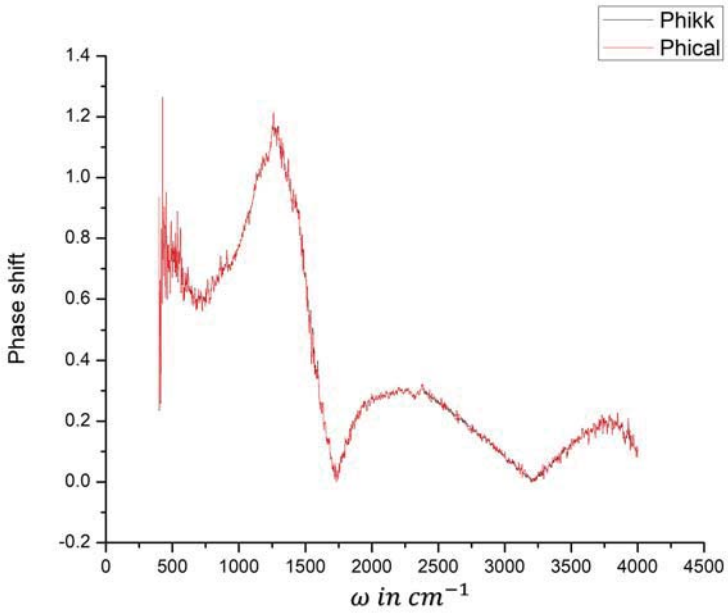

Figure 5.7: Phase shift of SiC deposited at 25 degree as function of ω

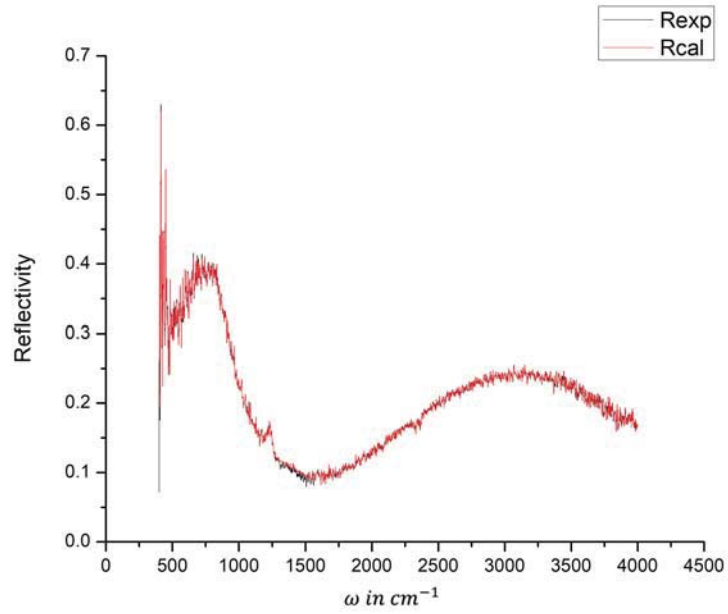

Figure 5.8: Reflectivity of SiC deposited at 600 degree as function of ω

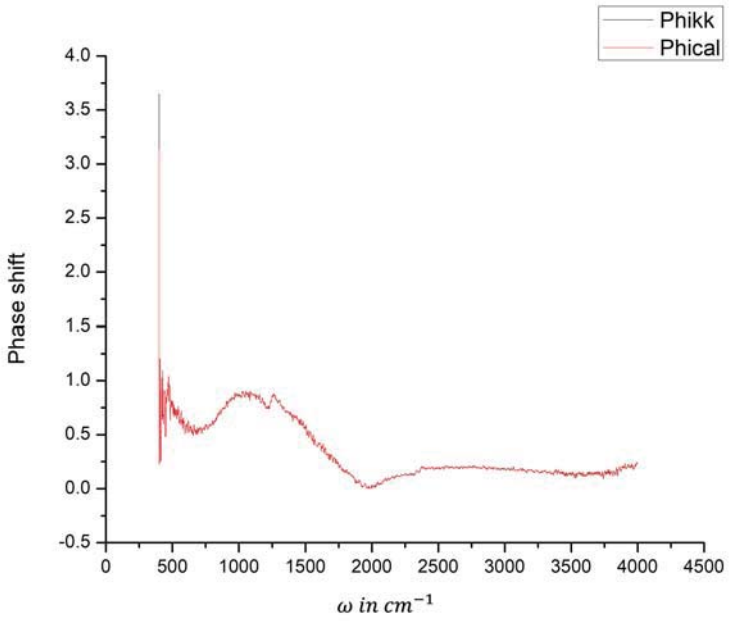

Figure 5.9: Phase shift of SiC deposited at 600 degree as function of ω

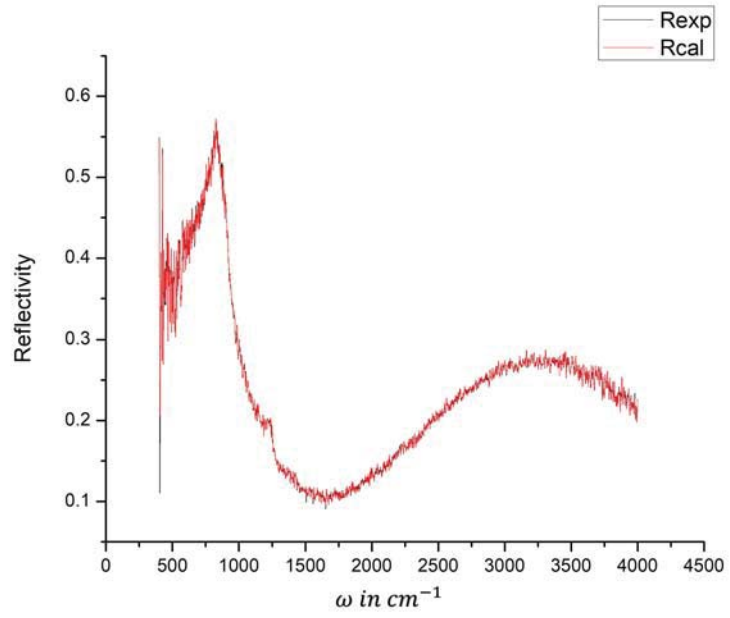

Figure 5.10: Reflectivity of SiC deposited at 900 degree as function of ω

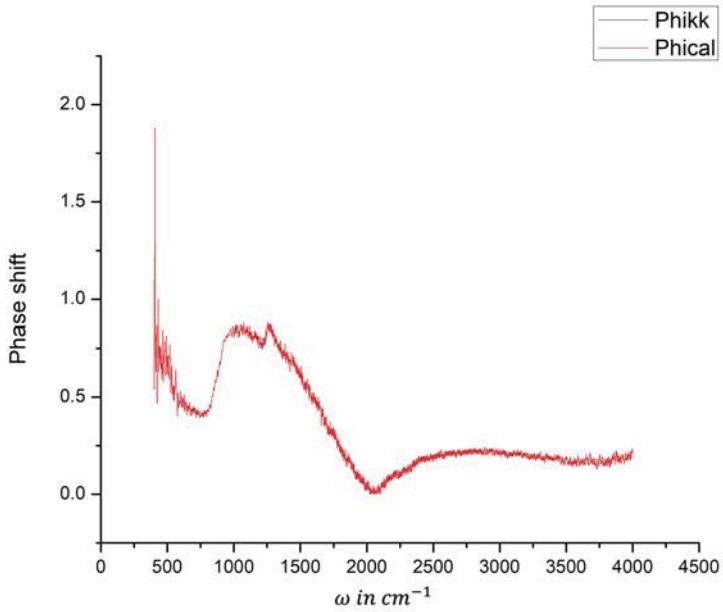

Figure 5.11: Phase shift of SiC deposited at 900 degree as function of ω

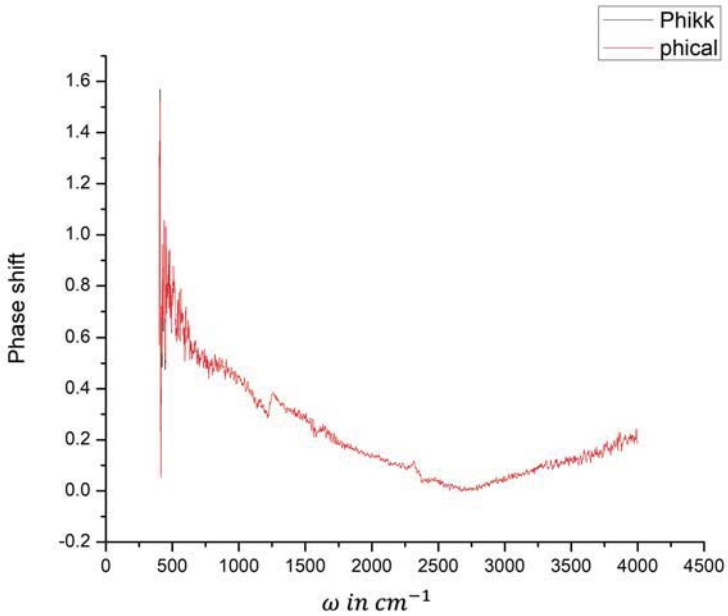

Figure 5.12: Reflectivity of SiC deposited at 700 degree as function of ω

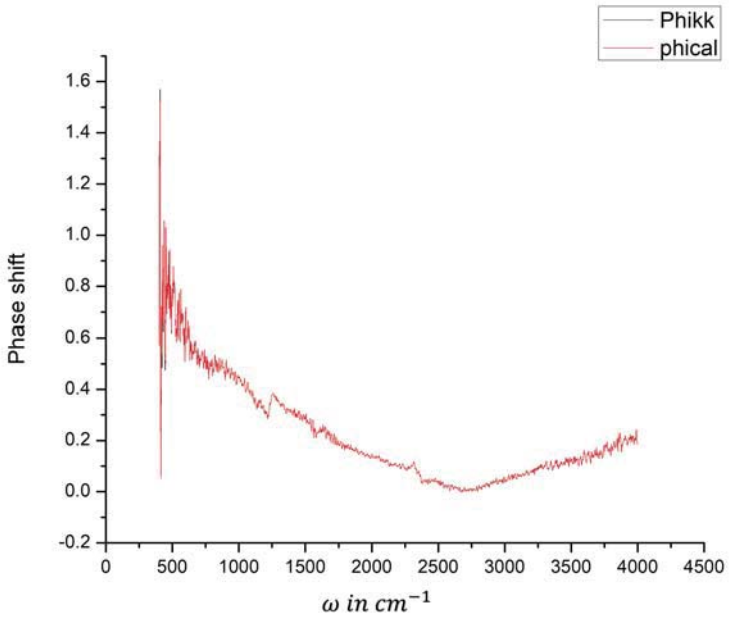

Figure 5.13: Phase shift of SiC deposited at 700 degree as function of ω

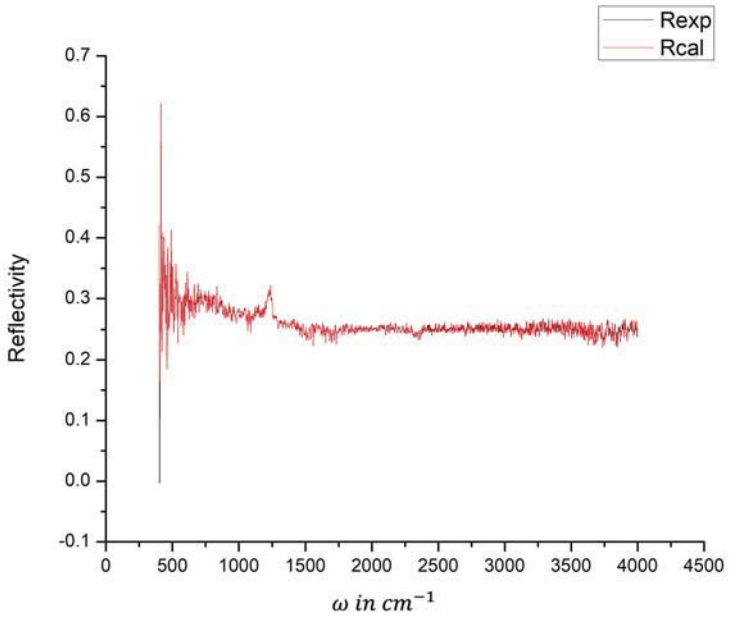

Figure 5.14: Reflectivity of SiC deposited at 900 degree as function of ω

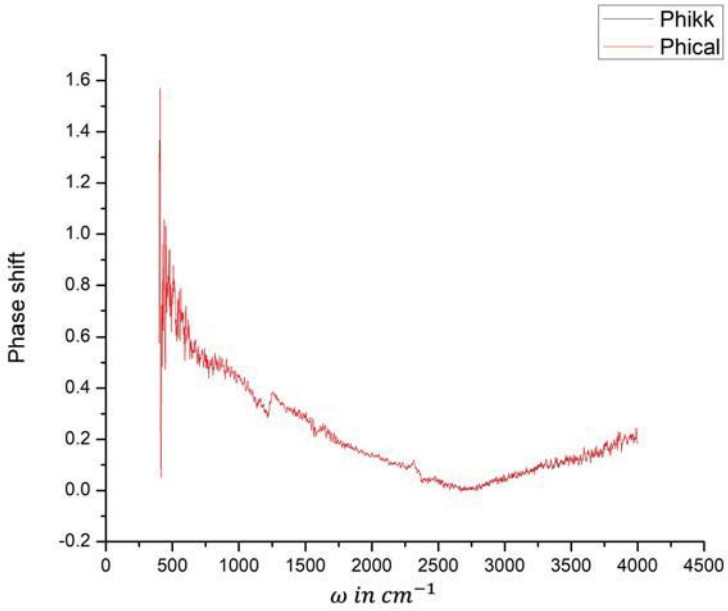

Figure 5.15: Phase shift of SiC deposited at 900 degree as function of ω

From the above figures, we see that the recalculated reflectivity **R** and phase shift ϕ agree with less than 1% with the experimental ones. Thus, by calculating back the reflectivity and phase shift, we are regenerating the experimental results. Thus, our results for the dielectric properties for our samples are true.

Conclusion

This work has been dedicated to develop an experimental technique for the measurement of the complex infrared dielectric function of a broad range of thin films deposited on a substrate.

In the first chapter, we present Maxwell's theory in its entirety, as well as the laws governing the propagation of electromagnetic waves in a polar dielectric. Special attention is given to the description of the behavior of electric and magnetic fields in dielectrics. This chapter should provide the necessary information on the interaction between light and matter.

In the second chapter, we present the experimental techniques used in this work. We provide a narrative description of the Pulsed Laser Deposition (PLD) growth technique that has been used to deposit amorphous silicon carbide films on silicon and the Raman spectroscopy technique that has been used to examine the crystallinity of the grown samples.

In the third chapter, we present the Fourier Transform Infrared Spectrometer (FTIR) used in this work. We also present the characteristics of this technique which make it the tool of choice for probing the complex dielectric functions of materials. We also present some results obtained from a reference sample showing the accuracy of this technique.

In the fourth chapter, we present a detailed theory on the reflection of light from a multilayer system. Then, we provide a description of the transfer matrix method for the calculation of Fresnel coefficients and its application for the evaluation of reflectance. In addition, we describe an approach, based on the combination of Fresnel theory and Kramers-Kronig conversion theorem, for the analysis of the infrared reflectance spectrum of a multilayer system and the derivation of the complex infrared dielectric function of a specific layer of the system.

In the fifth chapter, We use the technique developed to deduce the complex infrared dielectric function of amorphous silicon carbide thin films deposited on silicon at different temperatures and pressure levels using the pulsed laser deposition (PLD) growth technique. We show that the growth temperature does not have a significant effect on the dielectric properties of the amorphous films. However, the variation in pressure allows a substantial modification of the real and imaginary parts of the infrared complex dielectric function of the amorphous silicon carbide film.

Bibliography

[1] Sanford A Asher. Uv resonance raman spectroscopy for analytical, physical, and biophysical chemistry. part 2. *Analytical chemistry*, 65(4):201A–210A, 1993.

[2] B Jayant Baliga. *Fundamentals of power semiconductor devices*. Springer Science & Business Media, 2010.

[3] M Balooch, RJ Tench, WJ Siekhaus, MJ Allen, AL Connor, and DR Olander. Deposition of sic films by pulsed excimer laser ablation. *Applied physics letters*, 57(15):1540–1542, 1990.

[4] MA Capano, SD Walck, PT Murray, D Dempsey, and JT Grant. Pulsed laser deposition of silicon carbide at room temperature. *Applied physics letters*, 64(25):3413–3415, 1994.

[5] Michael A Capano. Time-of-flight analysis of the plume dynamics of laser-ablated 6h-silicon carbide. *Journal of applied physics*, 78(7):4790–4792, 1995.

[6] Y Catherine and G Turban. Infrared absorption of hydrogenated amorphous si c and ge c films. *Thin Solid Films*, 70(1):101–104, 1980.

[7] Ming Y Chen and P Terrence Murray. Deposition and characterization of sic and cordierite thin films grown by pulsed laser evaporation. *Journal of materials science*, 25(11):4929–4932, 1990.

[8] A Declémy, E Oliviero, MF Beaufort, JF Barbot, ML David, C Blanchard, Y Tessier, and E Ntsoenzok. An ir-reflectivity and x-ray diffraction study of high energy he-ion implantation-induced damage in 4h–sic. *Nuclear Instruments and Methods in Physics Research Section B: Beam Interactions with Materials and Atoms*, 186(1-4):318–323, 2002.

[9] D Dijkkamp, T Venkatesan, XD Wu, SA Shaheen, N Jisrawi, YH Min-Lee, WL McLean, and Mark Croft. Preparation of y-ba-cu oxide superconductor thin films using pulsed laser evaporation from high t c bulk material. *Applied Physics Letters*, 51(8):619–621, 1987.

[10] Philippe Djemia, Yves Roussigné, Guy F Dirras, and Kamili M Jackson. Elastic properties of β-sic films by brillouin light scattering. *Journal of applied physics*, 95(5):2324–2330, 2004.

[11] MA El Khakani, M Chaker, ME O'Hern, and WC Oliver. Linear dependence of both the hardness and the elastic modulus of pulsed laser deposited a-sic films upon their si–c bond density. *Journal of applied physics*, 82(9):4310–4318, 1997.

[12] A Fissel, U Kaiser, B Schröter, W Richter, and F Bechstedt. Mbe growth and properties of sic multi-quantum well structures. *Applied surface science*, 184(1-4):37–42, 2001.

[13] AM Fox. Optical properties of solids, ser, 2001.

[14] Charles Kittel, Paul McEuen, and Paul McEuen. *Introduction to solid state physics*, volume 8. Wiley New York, 1996.

[15] Derek Albert Long. Raman spectroscopy. *New York*, pages 1–12, 1977.

[16] Valerio Lucarini, Jarkko J Saarinen, Kai-Erik Peiponen, and Erik M Vartiainen. *Kramers-Kronig relations in optical materials research*, volume 110. Springer Science & Business Media, 2005.

[17] P Mandracci, A Chiodoni, G Cicero, S Ferrero, F Giorgis, CF Pirri, G Barucca, P Musumeci, and R Reitano. Heteroepitaxy of 3c–sic by electron cyclotron resonance-cvd technique. *Applied surface science*, 184(1-4):43–49, 2001.

[18] Pierre Masri. Silicon carbide and silicon carbide-based structures: the physics of epitaxy. *Surface science reports*, 48(1-4):1–51, 2002.

[19] S Nakashima and K Tahara. Raman scattering determination of structures for sic polytypes: quantitative evaluation with a revised model of lattice dynamics. *Physical Review B*, 40(9):6339, 1989.

[20] Jamey S Pelt, Matthew E Ramsey, and Steven M Durbin. Characterization of crystalline sic films grown by pulsed laser deposition. *Thin Solid Films*, 371(1-2):72–79, 2000.

[21] Sidney Perkowitz. *Optical characterization of semiconductors: infrared, Raman, and photoluminescence spectroscopy*. Elsevier, 2012.

[22] James W Robinson. *Practical handbook of spectroscopy*. CRC press, 1991.

[23] DA Skoog, F James Holler, and SR Crouch. Principles of instrumental analysis. thomson brooks. *Cole, Canada*, 2007.

[24] I Solomon. Amorphous silicon–carbon alloys: a promising but complex and very diversified series of materials. *Applied surface science*, 184(1-4):3–7, 2001.

[25] JW Strane, SR Lee, HJ Stein, ST Picraux, JK Watanabe, and JW Mayer. Carbon incorporation into si at high concentrations by ion implantation and solid phase epitaxy. *Journal of applied physics*, 79(2):637–646, 1996.

[26] Yuxia Wang, Jun Wen, Zhen Guo, Yeqing Tang, Honggao Tang, and Jianxin Wu. The preparation of single-crystal 4h-sic film by pulsed xecl laser deposition. *Thin Solid Films*, 338(1-2):93–99, 1999.

[27] H Wieder, M Cardona, and CR Guarnieri. Vibrational spectrum of hydrogenated amorphous si c films. *physica status solidi (b)*, 92(1):99–112, 1979.

[28] Pochi Yeh et al. *Optical waves in layered media*, volume 95. Wiley Online Library, 1988.

[29] C Yuan, AJ Steckl, J Chaudhuri, R Thokala, and MJ Loboda. Reduced temperature growth of crystalline 3c-sic films on 6h-sic by chemical vapor deposition from silacyclobutane. *Journal of applied physics*, 78(2):1271–1273, 1995.

[30] T Zehnder, A Blatter, and A Bächli. Sic films prepared by pulsed excimer laser deposition. *Thin Solid Films*, 241(1-2):138–141, 1994.